Journal of Hydrology 608 (2022) 127649

Contents lists available at ScienceDirect

Journal of Hydrology

journal homepage: www.elsevier.com/locate/jhydrol

Research papers

Pluvial flooding: High-resolution stochastic hazard mapping in urban areas by using fast-processing DEM-based algorithms

Luis Mediero [a,*], Enrique Soriano [a], Peio Oria [b], Stefano Bagli [c], Attilio Castellarin [d], Luis Garrote [a], Paolo Mazzoli [c], Jaroslav Mysiak [e], Stefania Pasetti [f], Simone Persiano [d], David Santillán [a], Kai Schröter [g]

[a] Department of Civil Engineering: Hydraulics, Energy and Environment, Universidad Politécnica de Madrid, 28040 Madrid, Spain
[b] Agencia Estatal de Meteorología (AEMET), 31004 Pamplona, Spain
[c] GECOsistema Srl, 47921 Rimini, Italy
[d] Department of Civil, Chemical, Environmental and Materials Engineering (DICAM), University of Bologna, 40136 Bologna, Italy
[e] CMCC Euro-Mediterranean Center on Climate Change, Ca' Foscari University of Venice, 30175 Venice, Italy
[f] MEEO Meteorological Environmental Earth Observation, 44123 Ferrara, Italy
[g] German Research Centre for Geosciences GFZ, Section Hydrology, Potsdam, Germany

ARTICLE INFO

This manuscript was handled by Marco Borga, Editor-in-Chief

Keywords:
Pluvial floods
Safer_RAIN
Flood hazard mapping
Rapid flood model
Urban areas
Bivariate return periods

ABSTRACT

Climate change and rapid expansion of urban areas are expected to increase pluvial flood hazard and risk in the near future, and particularly so in large developed areas and cities. Therefore, large-scale and high-resolution pluvial flood hazard mapping is required to identify hotspots where mitigation measures may be applied to reduce flood risk. Depressions or low points in urban areas where runoff volumes can be stored are prone to pluvial flooding. The standard approach based on estimating synthetic design hyetographs assumes, in a given depression, that the *T*-year design storm generates the *T*-year pluvial flood. In addition, urban areas usually include several depressions even linked or nested that would require distinct design hyetographs instead of using a unique synthetic design storm. In this paper, a stochastic methodology is proposed to address the limitations of this standard approach, developing large-scale ~ 2 m-resolution pluvial flood hazard maps in urban areas with multiple depressions. The authors present an application of the proposed approach to the city of Pamplona in Spain (68.26 km^2). The Safer_RAIN fast-processing algorithm based on digital elevation models (DEMs) is compared with the IBER 2D hydrodynamic model in four real storms by using 10-min precipitation fields. Precipitation recorded at rainfall-gauging stations was merged with continuous fields obtained from a meteorological radar station. Given the hydrostatic limitations of Safer_RAIN, the benchmarking results are adequate in terms of water depths in depressions. A long set of 10 000 synthetic storms that maintain the statistical properties of observations in Pamplona is generated. Safer_RAIN is used to simulate runoff response, and filling and spilling processes, in depressions for the 10 000 synthetic storms, obtaining the probability distribution of water depths in each cell. Maps of pluvial flood hazards are developed in the Pamplona metropolitan area for 10 return periods in the range from two to 500 years from such pixel-based series of simulated water depths. Bivariate return-period curves are estimated in a set of cells, showing that several storms can generate a given *T*-year pluvial flood with an increasing precipitation with storm duration that depends on the draining catchment soil characteristics. The methodology proposed is useful to develop maps of pluvial flood hazards in large multi-depression urban areas in reasonable computation times, identifying the main pluvial flood hotspots.

* Corresponding author.
E-mail addresses: luis.mediero@upm.es (L. Mediero), e.soriano@upm.es (E. Soriano), poriai@aemet.es (P. Oria), stefano.bagli@gecosistema.com (S. Bagli), attilio.castellarin@unibo.it (A. Castellarin), l.garrote@upm.es (L. Garrote), paolo.mazzoli@gecosistema.com (P. Mazzoli), jaroslav.mysiak@cmcc.it (J. Mysiak), pasetti@meeo.it (S. Pasetti), simone.persiano@unibo.it (S. Persiano), david.santillan@upm.es (D. Santillán), kai.schroeter@gfz-potsdam.de (K. Schröter).

https://doi.org/10.1016/j.jhydrol.2022.127649
Received 28 May 2021; Received in revised form 15 February 2022; Accepted 18 February 2022
Available online 23 February 2022

1. Introduction

Pluvial floods are usually generated by high-intensity and short-duration storms. Climate change projections point to an increase in the intensity and frequency of such extreme rainfall events (Kundzewicz et al., 2014). Furthermore, the expansion of urban areas and the increasing density of assets in cities have amplified the economic and human consequences associated with pluvial floods (Kaspersen et al., 2017; Bulti and Abebe, 2020). Pluvial flood hazards are usually assessed by using synthetic design storms (Krvavica and Rubinić, 2020) and two-dimensional (2D) hydrodynamic models. In this study, a stochastic methodology is proposed to estimate pluvial flood hazards in urban areas, overcoming some of the major limitations of deterministic approaches.

Synthetic design storms neglect the influence of both hyetograph shapes and spatial and temporal distributions of rainfall on water depths. In addition, such an approach assumes that the design storm for a given return period (T) generates the T-year pluvial flood. However, the T-year pluvial flood should be obtained by using a threshold in a variable that characterises flood hazardousness, such as water depths. Moreover, a high degree of uncertainty is associated with design hyetograph estimates, propagating it through rainfall-runoff simulations and pluvial flood hazard calculations, as catchment response times are usually estimated with empirical formulae that may not be valid in areas with different conditions from those of the regions used to obtain them, as well as the results can differ by up to 500 % depending on the formula used (Grimaldi et al., 2012; Gericke and Smithers, 2014; Tuyls et al., 2018). Consequently, urban drainage systems could be over- or under-estimated depending on the empirical formula used in each case. In addition, urban areas are usually composed of multiple depressions prone to pluvial flooding that can be even linked and nested. Each depression should be analysed independently when using an approach based on synthetic design storms, as varying catchment response times will lead to varying design hyetograph durations. Therefore, multiple simulations are required, increasing the complexity of pluvial flood hazard mapping at the scale of a city or municipality.

The limitations of the standard approach based on synthetic design hyetographs can be improved by using a stochastic analysis that considers the runoff response in a large set of storms, maintaining the statistical properties of real rainfall events observed in a given area. First, design hyetograph estimates are not required, as the complete probability distribution of water depths at any point will be obtained, addressing the assumption that the T-year storm generates the T-year pluvial flood. Second, the method can be applied to larger scales with multiple depressions, as it is independent of catchment response times at each depression. Third, a stochastic analysis avoids the uncertainties associated with catchment response time estimates by using empirical formulae. Consequently, a stochastic approach will be more adequate for pluvial flood hazard mapping in urban areas with multiple depressions. However, a rapid tool for simulating the water depths generated by a large set of storms is required for conducting such a stochastic approach.

2D hydrodynamic models are recognised to simulate pluvial floods in urban areas accurately (Henonin et al., 2013), based on solving the 2D shallow-water equations (SWEs) by using numerical methods. Therefore, they require high computation times. Furthermore, studies that use long sets of stochastic synthetic rainfall events are unusual for the delineation of pluvial flood hazard maps (Apel et al., 2016), as they are not affordable with the computation times required by 2D hydrodynamic models. Either simplified hydrodynamic models are used to reduce simulation times (Nuswantoro et al., 2016) or a reduced set of simulations are considered, such as 45 simulations (Simoes et al., 2015) and 160 simulations per probability (Apel et al., 2016).

Recently, computation times of 2D hydrodynamic models have been reduced with parallel computing techniques and graphic processing units (GPUs) (Guidolin et al., 2016), such as the LISFLOOD-FP and P–DWave models (Neal et al., 2009; Leandro et al., 2014); with topography simplifications by using sub-grid models (Yu and Lane, 2006; Neelz and Pender, 2007), and focusing on cells with low porosity values that tend to reduce computational efficiencies (Guinot et al., 2017; Bruwier et al., 2017). In addition, the solving complexity of 2D WSEs has been reduced by approximating or neglecting inertial and advection terms (Bates et al., 2010), and by using the cellular automata (CA) approach (Ghimire et al., 2013; Guidolin et al., 2016). However, such approaches would not be enough for conducting probabilistic analyses (Bernini and Franchini, 2013). Furthermore, artificial neural networks (ANNs) can be trained with a reduced set of 2D hydrodynamic model outputs (Bermúdez et al., 2018; Berkhan et al., 2019), though they are unable to interpolate between the rainfall events used to train the network; a set of hybrid models has been also developed (Chang et al., 2010; Pan et al., 2011), and approaches based on support vector machines have been offered (Lin et al., 2013; Jhong et al., 2017; Bermúdez et al., 2019). Therefore, a technique based on a 2D hydrodynamic model with short enough computation times and satisfactory results is not available yet.

Rapid flood models (RFMs) have been developed to shorten the computation times in contrast to 2D hydrodynamic models. They identify depressions from a digital elevation model (DEM), considering a set of storage reservoirs connected through links. The water balance equation is used to simulate depression filling and spilling processes (Bulti and Abebe, 2020). Therefore, high-resolution DEMs can be used with small pre-processing computation times. RFMs can reduce computation times to few minutes or even seconds, up to 1000 times compared with hydrodynamic models (Teng et al., 2007). Consequently, RFMs are adequate for conducting probabilistic analyses. Some RFMs are the Rapid Flood Spreading Model (RFSM) (Bernini and Franchini, 2013), the flood-connected domain calculation (FCDC) method (Zhang et al., 2014), the rapid urban flood inundation and damage assessment model (RUFIDAM) model (Jamali et al., 2018), and the cellular automata fast flood evaluation (CA-ffé) model (Jamali et al., 2019). Hierarchical filling-and-spilling algorithms (HFSAs) or puddle-to-puddle dynamic filling-and-spilling approaches (P2Ps) have been recognised as promising techniques for characterising pluvial floods (Chu et al., 2013; Zhang and Pan, 2014). In this respect, the Safer_RAIN tool has been developed recently (Samela et al., 2020). Safer_RAIN is a HFSA that can simulate detailed spatially distributed infiltration processes with the Green-Ampt model, supplying flood depths and extents.

Probabilistic approaches are more correct than deterministic approaches based on T-year design events, as design event estimates have significant uncertainties and 2D models are not perfect (Di Baldassarre et al., 2010). Probabilistic approaches based on continuous simulation needs a long period of rainfall time series (Nuswantoro et al., 2014). Semi-continuous simulation approaches have been proposed to reduce simulation times (Lawrence et al., 2014; Jamali et al., 2020). However, stochastic approaches can generate larger samples of storms that can extend the available time series of observed rainfall events.

In this study, a stochastic methodology is proposed to delineate probabilistic pluvial flood hazard maps across large urban areas and cities with ~ 2-m horizontal resolution. The fast-processing DEM-based Safer_RAIN algorithm (Samela et al., 2020) is used, benefiting from its computational efficiency and low runtimes, as well as from its ability to simulate spatially distributed infiltration processes. Therefore, the limited number of simulations that can be considered by using a 2D hydrodynamic model (Simoes et al., 2015; Apel et al., 2016) is overcome by using such a RFM. In addition, the Safer_RAIN algorithm does not need to be coupled to a rainfall-runoff model. The stochastic approach proposed can generate a long set of synthetic rainfall events with similar statistical properties to real rainfall events by using a methodology based on copulas, extending the usual length of rainfall time series utilised in continuous and semi-continuous approaches. In addition, the limitations of using a deterministic approach based on a single synthetic design storm (Krvavica and Rubinić, 2020) are improved by considering

such a large set of storms. The probability distribution of water depths is obtained in each cell of the domain. Furthermore, flood depths and extents for given return periods are estimated from the water depth series obtained in each cell. In addition, bivariate return-period curves are estimated, analysing the relationship between the variables that characterise storms and pluvial flood water depths in a given depression. The methodology has been applied to the Pamplona metropolitan area in Spain.

This study is structured as follows. Section 2 presents the case study and the models used in the analysis. Section 3 offers the methodology proposed for the delineation of pluvial flood hazard maps at municipality scales. Section 4 presents the application of the methodology to the case study of the Pamplona metropolitan area. Section 5 discusses the results and limitations of the methodology proposed. Section 6 summarises the main conclusions of the study.

2. Case study and models

First, this section presents the Pamplona metropolitan area case study, as well as the data available. Second, the models used are described: The Safer_RAIN algorithm, the 2D IBER hydrodynamic model, and the infiltration equation used to simulate rainfall losses.

2.1. Pamplona case study

Pamplona is located in the Navarre Region in the northern part of Spain (Fig. 1). The Pamplona metropolitan area is 68.26 km^2 and has around 335 000 inhabitants, including the municipalities of Barañáin, Burlada, Cendea de Olza, Cizur, Huarte, Orcoyen, Pamplona, Villava and Zizur Mayor (Fig. 2). It is subject to pluvial floods mainly in the summer months. The municipalities of Barañáin and Zizur Mayor have the highest pluvial flood losses according to the database provided by the Spanish *Consorcio de Compensación de Seguros* that compensates the damages produced by natural hazards in Spain. For the 20 July 2010 pluvial flood event that is the greatest in the Pamplona metropolitan area in the period 1996–2020, such a database supplies a total flood loss of 3.319 M€ updated to the year 2020. 70.7 % of the flood losses were concentrated in Zizur Mayor and Barañáin areas: 1.687 M€ in Zizur Maryor and 0.66 M€ in Barañáin and the closest postal code of Pamplona to Barañáin. Therefore, such areas have been selected for the Safer_RAIN benchmark activities described in Section 3.1.

The 2-m DEM considered in the study was supplied by the Spanish National Geographic Institute (*Instituto Geográfico Nacional*, IGN, in Spanish). Precipitation data at four gauging stations were supplied by the real-time Automatic Hydrological Information System (*Sistema Automático de Información Hidrológica*, SAIH, in Spanish) of the River Ebro Basin Authority, the Spanish State Meteorological Agency (*Agencia Estatal de Meteorología*, AEMET, in Spanish), the Regional Government of Navarre, and the *Universidad Pública de Navarra* (UPNA, in Spanish) (see Table 1).

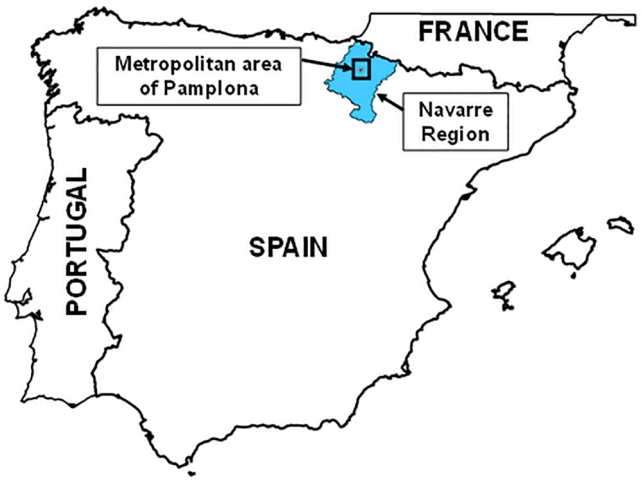

Fig. 1. Location of the Pamplona metropolitan area in Spain.

Three real pluvial flood events have been identified in the Barañáin and Zizur Mayor municipalities in recent years (Table 2). First, the day of occurrence of the main flood events in the Pamplona metropolitan area were extracted from the database supplied by the Spanish *Consorcio de Compensación de Seguros*. Such events can be either fluvial or pluvial. Therefore, the type of flood for each event was identified by checking streamflow and precipitation observations, as well as pieces of news in the *Diario de Navarra* newspaper. Finally, the three main pluvial flood events in the Pamplona metropolitan area were selected.

The return period for each event in Table 2 has been estimated from the intensity–duration–frequency (IDF) curve for the storm duration by using the total storm precipitation depth. The 20 July 2010 event had a rainfall of 42.6 mm and a peak intensity of 66.4 mm/h in 15 min at the rain-gauging station P1, with a return period estimate of 14.3 years. On 18 September 2019, two storms were identified: a 37.8 mm storm with a peak intensity of 74.4 mm/h in 10 min at the P4 station in the morning, which corresponds to a return period of 16.3 years, and a small-scale 25.9 mm storm with a peak intensity of 73.2 mm/h in 10 min at the P4 station in the afternoon associated with a return period of 4.37 years. The storm of 25 April 2020 was highly localised at the Barañáin municipality and characterised by using the precipitation fields described in Section 2.1.1, with a peak rainfall of 12 mm in 10 min in the area of Zizur Mayor and Barañáin.

2.1.1. Quantitative precipitation estimation fields in the Pamplona metropolitan area

Optimised and high-resolution quantitative precipitation estimations (QPEs) are required for identifying where localised heavy or torrential storms may take place, coping with pluvial flood events properly (Zhang et al., 2016). The combination of surface and remote sensing-based radar data can generate a merged product that reduces the errors obtained by using only either rain-gauging interpolation or radar data, as radar data cover large areas and capture better the spatial variability of rainfall fields (McKee and Binns, 2016). A variety of techniques is available for the merging process (Ochoa-Rodríguez et al., 2019), though geostatistical methods provide the most satisfactory results, such as the kriging with external drift (KED) technique (Sharon and Gaussiat, 2015). KED is an extension of kriging that uses external variables, in this case radar QPEs, as auxiliary information in the interpolation process. Linear weights employed in the interpolation of point-gauge values are further constrained by the spatial association between radar and rain-gauge values. In addition, the real-time semivariogram model is obtained with real-time radar data, describing the spatial correlation between data.

QPEs with a 10-min time step are obtained in the metropolitan area of Pamplona for the four storms included in Table 2 (Fig. 3). Precipitation recorded at automatic weather stations (AWSs) from different organisms, such as AEMET, the Regional Government of Navarre, and crowdsourced networks, are merged with raw continuous fields obtained from the AEMET Zaragoza regional radar that supplies 10-min surface rainfall intensity (SRI) based on the 0.5° elevation radar reflectivity by using the C band (5.6 GHz). The number of rain-gauging stations used in each event depends on the data availability. Crowdsourced real-time rainfall data is acquired from the Weather Underground network that is fed by a global community of people connecting data from personal weather stations. For example, rainfall data was available for 10 crowdsourced stations in the 25 April 2020 event. Radar data quality is good enough, despite the signal attenuation and the high beam elevation, as Zaragoza is located 150 km from Pamplona. Furthermore, raw radar data are post-processed with ground clutter identification, correction for vertical profile of reflectivity (VPR) and reflectivity-to-

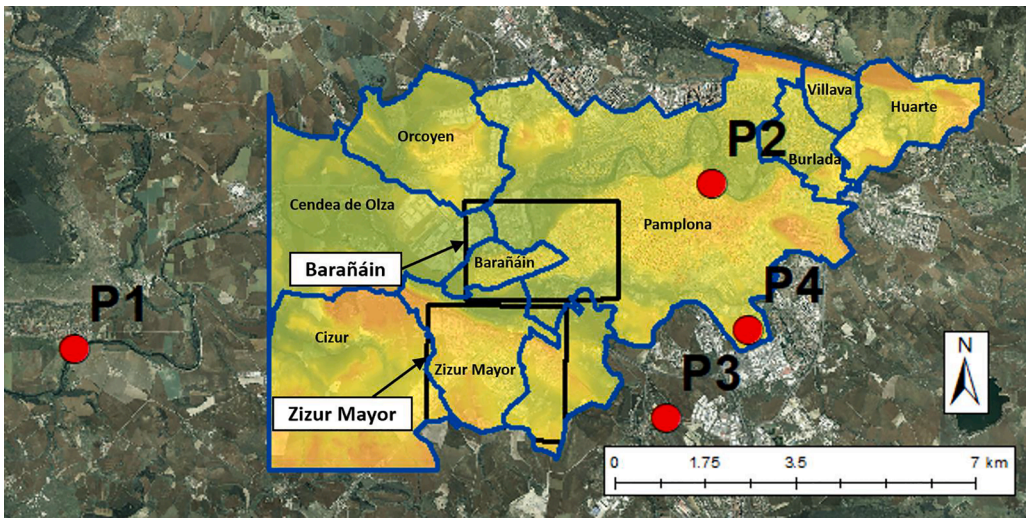

Fig. 2. Metropolitan area of Pamplona with the location of the municipalities (blue lines), the extents of the Barañáin and Zizur Mayor case studies for the benchmarking activities (black squares), and location of the four rain-gauging stations considered in the study (red points). Source of background layer: IGN.

Table 1
Rain-gauging stations considered in the study.

Code	Location	Period	Time step (min)	Institution
P1	Echauri	1997–2020	15	SAIH of the River Ebro Basin Authority
P2	Pamplona GN	1999–2018	10	Regional Government of Navarre
P3	Noáin Airport	2010–2020	10	AEMET
P4	Pamplona UPNA	2004–2020	10	UPNA

Table 2
Rainfall, duration, and peak intensity of the four storms selected as case studies. The four values included in each cell correspond to the observations at P1, P2, P3 and P4 rainfall-gauging stations of Table 1.

Date	Rainfall (mm)	Duration (hour)	Peak intensity (mm/h)
20 July 2010	42.6/7.83/ 6.8/4.8	1.75/2.17/ 1.5/1.33	66.4/26.6/ 23.4/14.4
18 September 2019 (Storm 1 – morning)	15.6/19.9/ 31.7/37.8	2.25/2.33/ 2.33/2.17	26.4/42/58.8/ 74.4
18 September 2019 (Storm 2 – afternoon)	0.8/25.9/0.2/ 11.4	1/1.33/0.33/2	0.8/73.2 /0.6/ 30
25 April 2020	1.2/9.1/3.8/ 4.2	1.25/3.2/ 2.33/2.67	1.6/19.2/4.2/ 3.6

rain-rate conversion by using the Marshall–Palmer Z–R relationship (Marshall and Palmer, 1948). While radar fields are generated with a time step of 10 min, rainfall gauging stations collects data with a time step of five to ten minutes. Therefore, at-site rainfall data are synchronised with radar scan time, minimising the uncertainty from signal mismatches by using advection schemes (Tabary, 2007; Shapiro et al., 2010).

In addition, the linear relationship between primary and auxiliary variables in KED may not remain valid for the whole range of rainfall intensities, especially in the case of heavy precipitation events. The expected value of the primary variable is the estimated precipitation. KED adds information about the secondary or auxiliary fields that may contribute to a better prediction of the geospatial field of precipitation, as they are related to the primary variable. The radar-based SRI data are utilised as auxiliary fields. In addition, logarithmic transformations of the variables are tested to improve the results in the case of dominant non-linear relationships between primary and secondary variables, such as in heavy or torrential storms. Therefore, QPE fields are selected among four options automatically via cross-validation in real time: (i) only SRI-based QPE; (ii) KED with linear variables in both the primary and auxiliary variables; (iii) KED with the logarithm of the primary variable; and (iv) KED with logarithms in both variables.

2.2. Models

The Safer_RAIN algorithm (Samela et al., 2020) has been developed within the SaferPlaces project. Safer_RAIN is implemented in the SaferPlaces platform (https://platform.saferplaces.co), in order to assess pluvial, fluvial and coastal flood hazard and risk in urban environments under current and future climates.

In this paper, Safer_RAIN is used to estimate water depths and flood extensions in the stochastic methodology. In addition, the 2D hydrodynamic IBER model (Bladé et al., 2014) was used for the Safer_RAIN benchmarking with the four storms selected in Table 2. Both models consider the Green-Ampt infiltration equation for simulating rainfall losses (Green and Ampt, 1911).

2.2.1. Safer_RAIN algorithm

Safer_RAIN is a fast-processing HFSA that identifies pluvial-flooded areas on the basis of nested surface depressions extracted from high-resolution LIDAR DEMs and a given rainfall depth, considering spatially distributed rainfall inputs and infiltration processes (Samela et al., 2020). Its main simplifying assumption consists of neglecting overland flow dynamics. Consequently, net-rainfall volumes accumulate in the system of nested depressions according to their capacity and hierarchical structure.

Safer_RAIN consists of two main steps. In the first, DEM pre-processing aims to identify the hierarchy-tree of nested depressions that defines the sequence of depression filling and spilling, as well as the filling volumes in each one. In the second, depression flooding identifies flooded areas and simulates corresponding water depths. The flooding phase implemented in Safer_RAIN is original in three senses. In the first, a bottom-up level-set method is applied for quantifying partial filling in nested higher-level depressions (for more details, see Samela et al., 2020). In the second, either uniform or spatially variable (i.e. gridded) rainfall depths can be used as input rainfall volume. And in the third, infiltration losses can be simulated with a pixel-based adaptation of the event-based Green-Ampt infiltration model (Green and Ampt, 1911).

Samela et al. (2020) reported the first applications of Safer_RAIN to

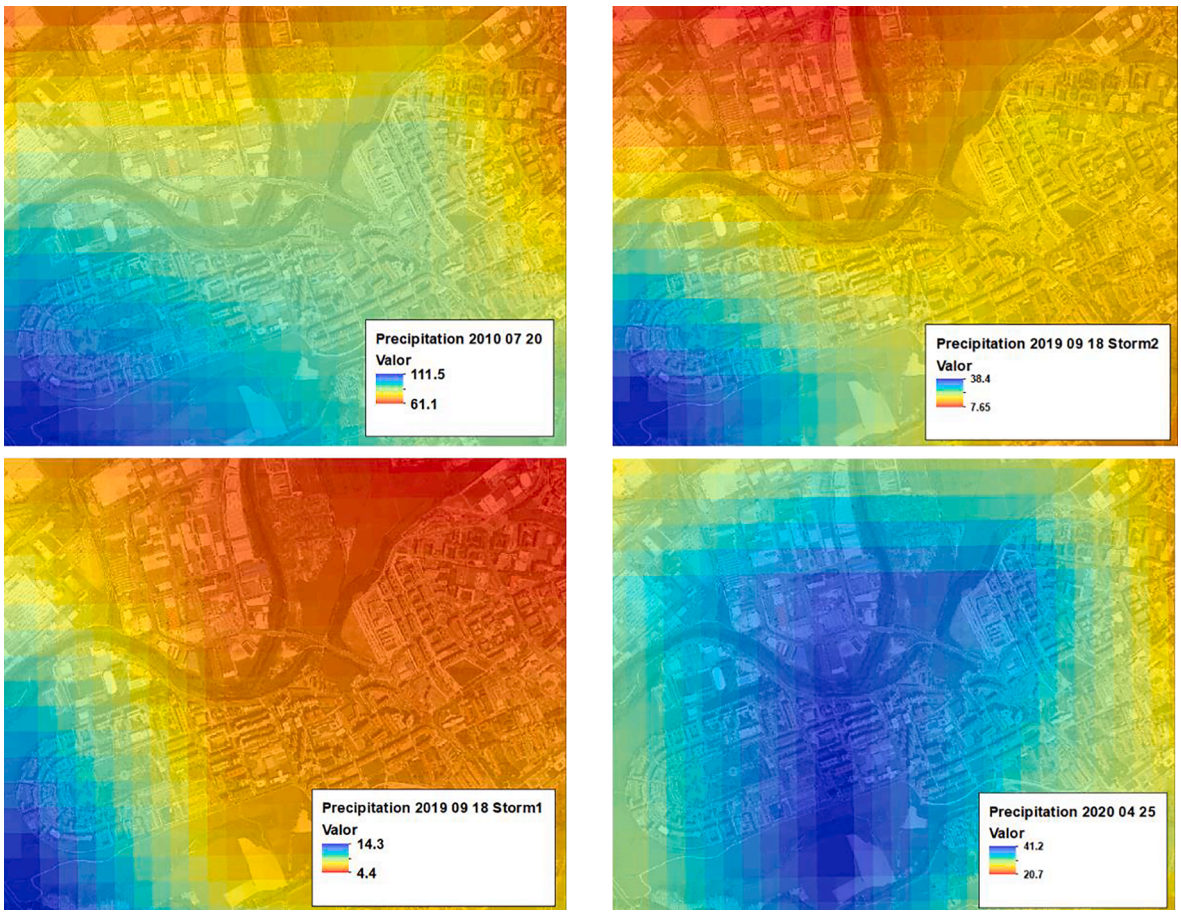

Fig. 3. Spatial distribution of cumulative rainfall depths (mm) in the Barañáin municipality for the four storms selected as case studies.

two case studies in northern Italy, where it was benchmarked with a 2D hydrodynamic model. The results showed an agreement of 53 % for the flooded area in Lignano Sabbiadoro and accuracy values in the range of 0.96–0.99 with the accuracy correlation coefficient (ACC) in Rimini. These applications highlighted the fast computation of flooded areas guaranteed by Safer_RAIN, as the pre-processing phase can be run once for a given study area. In addition, the results revealed the effectiveness in identifying pluvial-hazard hotspots with spatially distributed rainfall and different land-use scenarios, though the simulations are hydrostatic and Safer_RAIN cannot consider flow dynamic effects.

2.2.2. 2D IBER hydrodynamic model

Flood extensions and water depths are obtained for the four storms shown in Table 2 by using numerical simulations with the IBER code (Bladé et al., 2014; Cea et al., 2007). IBER is free software that solves the 2D depth-averaged SWEs by using a finite volume scheme, with the domain being discretized with both structured and unstructured triangular or quadrilateral elements (Cueto-Felgueroso et al., 2019; Santillán et al., 2020). It solves the mass conservative equation (Eq. (1)) and the momentum balance equations in conservative form with source terms (Eq. (2) and Eq. (3)):

$$\frac{\partial h}{\partial t}+\frac{\partial hV_x}{\partial x}+\frac{\partial hV_y}{\partial y}=0 \tag{1}$$

$$\frac{\partial hV_x}{\partial t}+\frac{\partial}{\partial x}\left(hV_x^2\right)+\frac{\partial}{\partial y}\left(hV_xV_y\right)=-gh\frac{\partial z_b}{\partial x}-\frac{\tau_{b,x}}{\rho} \tag{2}$$

$$\frac{\partial hV_y}{\partial t}+\frac{\partial}{\partial x}\left(hV_x^2\right)+\frac{\partial}{\partial y}\left(hV_yV_x\right)=-gh\frac{\partial z_b}{\partial x}-\frac{\tau_{b,y}}{\rho} \tag{3}$$

where h is the water depth, V_i is the depth average velocity along the ith direction, ρ is the water density, z_b is the height of the river bed, $\tau_{b,i}$ is the bed friction term along the ith direction, and g is the gravitational acceleration.

2.2.3. Green-Ampt infiltration equation

The Green-Ampt infiltration equation is considered in both Safer_RAIN and IBER models. They consider a pixel-based adaptation of the event-based Green-Ampt infiltration model (Green and Ampt, 1911) that assumes that water infiltrates into relatively dry soil as a sharp wetting front, computing the infiltration or rainfall loss with Eq. (4).

$$f_i=K_s\left(1+\frac{(\varphi-\theta_i)\Psi}{F_t}\right) \tag{4}$$

where f_t is the infiltration rate or rainfall loss rate at time step t (mm/h), K_s is the saturated hydraulic conductivity (mm/h), φ is the soil porosity (-), θ_i is the initial water content (-), Ψ is the wetting front suction (mm), and F_t is the cumulative infiltration or rainfall loss at time step t (mm).

Water infiltrates in soils until the rainfall rate exceeds the soil-limited infiltration rate. Therefore, the time to ponding (t_p) is considered. Specifically, in a given pixel with homogeneous land-cover and soil-type characteristics, the Green-Ampt module applied in Safer_RAIN computes the overall infiltration depth F at the end of the rainfall event ($t=d$) with Eq. (5).

$$F=\begin{cases} i\cdot d, & \text{if } d\le t_p \\ i\cdot t_p+K_s\cdot\left(d-t_p\right)+\Psi\cdot\Delta\theta\cdot\ln\left(\dfrac{\Psi\cdot\Delta\theta+F}{\Psi\cdot\Delta\theta+i\cdot t_p}\right), & \text{if } d>t_p \end{cases} \tag{5}$$

where i is rainfall intensity (mm/h), $\Delta\theta$ is defined as $\varphi-\theta_i$, d is the

storm duration, and t_p can be computed with Eq. (6).

$$t_p = \begin{cases} \infty, & if\ i \le k \\ \dfrac{\Psi \cdot \Delta\theta \cdot K_s}{i \cdot (i - K_s)}, & if\ i > k \end{cases} \quad (6)$$

Land-use and lithology layers have been used to identify soil types in the Pamplona metropolitan area. Values of the Green-Ampt parameters for each soil type have been obtained from literature based on previous experiences (see e.g., Chow et al., 1988).

3. Methodology

The methodology consists of six steps (Fig. 4). The first step of the methodology consists of benchmarking the Safer_RAIN algorithm with the IBER model in the Barañáin and Zizur Mayor municipalities by using the precipitation fields for the four storms selected in Table 2. The second involves identifying a set of real rainfall events that can generate pluvial flood events in Pamplona extracted from the time series recorded at the four gauging stations considered in the study. In the third, the copula-based stochastic generator of rainfall storms that maintain the statistical characteristics of the real storms identified in the previous step is described. In the fourth, the methodology to estimate *T*-year water depths in each cell of the Pamplona metropolitan area is offered. In the fifth, the methodology to compare the results of the stochastic methodology with the standard approach is presented. In the sixth, and last step, the methodology to assess the uncertainty of *T*-year water depth estimates is shown.

3.1. Benchmarking of Safer_RAIN

The Safer_RAIN algorithm outputs are benchmarked in the Barañáin and Zizur Mayor municipalities (Fig. 2) with the 2D hydrodynamic IBER model. The 10-min QPE fields generated for the four storms included in Table 2 are used as input data in both models. There are no observations available about flood extents and water depths for such four pluvial events. Therefore, the outputs of the 2D hydrodynamic model are considered as the gold standard truth. For the sake of simplicity, the urban drainage system is not considered in either model.

While IBER is a 2D hydrodynamic model, the Safer_RAIN tool is hydrostatic and can only simulate water depths and flood extents in depressions where water is stored. Therefore, maximum water depths simulated by IBER cannot be used in the comparison and the IBER model is run until six hours after the end of the storm when hydrodynamic processes are expected to be smoothed. Water depth outputs of the IBER model at six hours after the end of the storm are compared with outputs of the Safer_RAIN algorithm.

The errors between the models are quantified by using a set of objective functions (Bennett et al., 2013; Falter et al., 2013; Berkhahn et al., 2019; Samela et al., 2020). A given cell is considered as flooded when its water depth is equal or greater than 10 cm. First, the bias and root-mean-square error (RMSE) between water depths in the flooded area are calculated. Second, the critical success index (CSI) is used to quantify the agreement between the two models in terms of flood extents, measuring the fraction of cells that were correctly modelled and penalizing both misses and false alarms. The probability of detection, hit rate or true positive rate (R_{TP}) calculates the number of flooded agreements among the flooded areas in the gold standard truth simulation, quantifying the model sensitivity. The true negative rate (R_{TN}), or specificity, counts the number of non-flooded agreements among the non-flooded cells in the benchmark simulation. The accuracy correlation coefficient (ACC) quantifies the number of correct assessments between the simulations. Lastly, the Mathews correlation coefficient (MCC) measures the correlation between the binary classification in the simulations.

$$CSI = \frac{TP}{TP + FP + FN} \quad (7)$$

$$R_{TP} = \frac{TP}{TP + FN} \quad (8)$$

$$R_{TN} = \frac{TN}{TN + FP} \quad (9)$$

$$ACC = \frac{TN + TP}{TN + TP + FN + FP} \quad (10)$$

$$MCC = \frac{TP \cdot TN - FP \cdot FN}{\sqrt{(TP + FP)(TP + FN)(TN + FP)(TN + FN)}} \quad (11)$$

where *TP* (true positive or hints) is the number of cells where both models delineate them as flooded, *FP* (false positive or false alarms) is the number of cells that Safer_RAIN simulates as flooded and IBER simulates as non-flooded, *TN* (true negative) is the number of cells

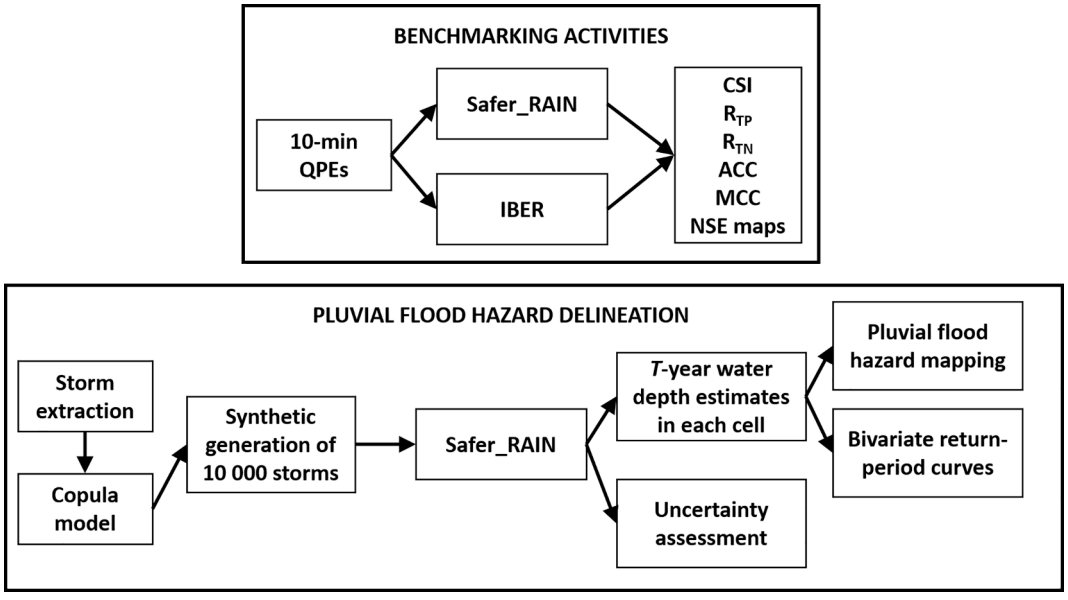

Fig. 4. Methodology flowchart.

where both models agree in delineating them as non-flooded, and *FN* (false negative or misses) is the number of cells that Safer_RAIN simulates as non-flooded and IBER simulates as flooded.

CSI can adopt values of between zero and one. While a value of one points to a perfect simulation of Safer_RAIN, a value of zero indicates that none of the flooded cells simulated by Safer_RAIN are flooded in the IBER simulation. MCC can provide values between −1 that would mean a complete disagreement between Safer_RAIN and IBER and one that would point to a perfect simulation of Safer_RAIN. A value of zero indicates that the Safer_RAIN output would not be better than a random prediction.

In addition, the Nash-Sutcliffe efficiency coefficient (NSE) is calculated in each cell for the four pluvial flood events (Eq. (12)).

$$NSE = 1 - \frac{\sum_{i=1}^{n}\left(WD_{Safer\_RAIN,i} - WD_{IBER,i}\right)^2}{\sum_{i=1}^{n}\left(WD_{IBER,i} - \overline{WD}_{IBER}\right)^2} \quad (12)$$

where $WD_{Safer\_RAIN,i}$ is the water depth simulated by Safer_RAIN in the *i*th pluvial flood event, $WD_{IBER,i}$ is the water depth simulated by IBER in the *i*th pluvial flood event, $\overline{WD}_{IBER}$ is the mean value of the water depths simulated by IBER in the *n* flood events, and *n* is the number of flood events considered. In cells with a negative value of NSE, $\overline{WD}_{IBER}$ would be a better prediction than the Safer_RAIN output.

NSE has been calculated in the cells with $\overline{WD}_{IBER}$ greater than 0.1 m, as smaller values of $\overline{WD}_{IBER}$ can lead to an excessively small value of the denominator in Eq. (12), resulting in unusual high negative values of NSE, despite small differences between Safer_RAIN and IBER simulations.

3.2. Extraction of rainfall events

Rainfall events that can drive pluvial floods in the metropolitan area of Pamplona are identified. In this study, a peak-over-threshold (POT) approach is selected to consider a larger set of rainfall events that exceed a given threshold, regardless of when they occurred. In a POT series, the arrival of rainfall events that exceed the threshold can be characterised by a Poisson process (Madsen et al., 1997) (Eq. (13)).

$$P(m = k) = \frac{\lambda^k}{k!}e^{-k} \quad (13)$$

where $P(m = k)$ is the probability of having a number of exceedances *m* equal to an integer number *k* in a given period of *t* years, *k* is an integer number equal or higher than zero ($k = 0, 1, 2, \ldots$), and λ is the mean annual number of exceedances that is obtained with Eq. (14).

$$\lambda = \frac{m}{t} \quad (14)$$

where *m* is the number of exceedances over the threshold in a period of *t* years.

Pluvial floods are generated by high-intensity events in short durations. Consequently, long events with high rainfall amounts and low intensities should not be considered in this analysis. The POT threshold for pluvial floods is usually selected in terms of rainfall intensity. The Extreme-Rainfall Alert (ERA) establishes a threshold that depends on the storm duration: 30 mm in 1 h, 40 mm in 3 h, and 50 mm in 6 h (Hurford et al., 2012). Apel et al. (2016) selected a threshold of 18 mm in 1 h. Blanc et al. (2012) identified a decreasing mean rainfall intensity threshold with storm duration, from around 3 mm/h in 1 h to 2 mm/h in 10–24 h. Mailhot et al. (2013) selected a threshold between 2 and 10 mm in 30 min depending on the calendar day. In this study, a threshold of 10 mm in 30 min that corresponds to a rainfall intensity of 20 mm/h is selected, considering the characteristics of the storms that have generated pluvial floods in Pamplona (Table 2).

3.3. Stochastic generation of rainfall events

A stochastic methodology to generate synthetic rainfall events that maintain the statistical properties of the rainfall events identified in Section 3.2 is presented. Storms are characterised by rainfall depth and duration, which are the input data of the Safer_RAIN algorithm. Synthetic pairs of rainfall depth and storm duration can be generated by using bivariate copulas (Palla et al., 2018). In this exploratory analysis, for the sake of simplicity some simplifications have been introduced. Though Safer_RAIN can consider spatial distributions of rainfall and QPE fields have been considered in the benchmarking analysis to simulate four real pluvial flood events accurately, precipitation fields have not been considered in the stochastic rainfall generator to reduce the computation times required for calibrating the rainfall generator, simulating the precipitation fields, and running the Safer_RAIN algorithm. Therefore, the stochastic method will consider uniform rainfalls and durations in the Pamplona metropolitan area and a longer set of 10 000 synthetic rainfall events will be examined in the study.

The procedure consists of two steps. In the first, the observed storms that exceed the threshold of 10 mm in 30 min at the four rainfall-gauging stations are aggregated in a unique synthetic gauging site, in order to obtain a larger time series and reduce estimate uncertainties. This aggregation is justified considering that the distance between the rainfall gauging sites is small enough (Fig. 2) to assume that they have similar characteristics. In addition, gauging sites are far enough to record varying storm rainfall depths, intensities and durations for a given pluvial flood event, given that such events are characterised by a high spatial variability.

In the second, a bivariate approach is used to generate synthetic rainfall events. In this case, the first step consists of fitting the marginal distributions of rainfall depth and duration for the aggregated set of storms that exceed the threshold. The magnitude of exceedances over a threshold are usually characterised by a generalised Pareto (GP) distribution function (Madsen et al., 1997; Lang et al., 1999), as it is a limiting distribution for a series of values that exceed a threshold and it has threshold stability (Martins and Stedinger, 2001). The parameters of the GP distribution are estimated by using the L-moments method (Hosking and Wallis 1993; 1997).

The second step of the bivariate approach consists of using a copula to characterise the dependence between storm rainfall depths and durations (Sklar, 1959). In this study, three Archimedean copula families are considered: Clayton, Frank, and Gumbel. In addition, the Gumbel copula belongs to the extreme value family. The Cramér-von Mises statistic (S_n) is selected as the goodness-of-fit test to identify the copula that can represent better the dependence structure between rainfall depths and durations (Eq. (15)), as Genest et al. (2009) found that S_n led to the best results for all copula models (Requena et al., 2013).

$$S_n^i = \sum_{j=1}^{n_i}\left\{C_n^i\left(\frac{R_{ij}}{n_i+1}, \frac{S_{ij}}{n_i+1}\right) - C^i\left(\frac{R_{ij}}{n_i+1}, \frac{S_{ij}}{n_i+1}; \widehat{\theta}_{cop}^i\right)\right\}^2, i = 1:N, \quad (15)$$

where $C_n^i(u_1, u_2)$ is the empirical copula at site *i*, R_{ij} and S_{ij} are the ranks associated with x_{ij} and y_{ij}, $\widehat{\theta}_{cop}^i$ are the estimated parameters of the fitted parametric copula C^i at site *i*; and n_i the record length at site *i*. $C_n^i(u_1, u_2)$ is expressed by Eq. (16).

$$C_n^i(u_1, u_2) = \frac{1}{n_i}\sum_{j=1}^{n_i} 1\left(\frac{R_{ij}}{n_i+1} \le u_1, \quad \frac{S_{ij}}{n_i+1} \le u_2\right); \quad u_1, u_2 \in [0,1]; \quad i = 1:N, \quad (16)$$

where **1**(E) is the indicator function of the set E (valued 1 inside E or 0 outside), and *n* is the observed record length.

In addition, the *p*-value associated with a given goodness-of-fit test is crucial in determining if a given copula model is suitable to characterise

the dependence between two variables (Genest and Rémillard, 2008). Therefore, first the p-value is used to reject a given copula model when it is smaller than 0.05. Then, the value of the S_n statistic is used to select the best copula among the non-rejected ones. The lowest value of S_n indicates the best fitting to observations (Salvadori and De Michele, 2011). Consequently, the selected copula should have the lowest value of S_n with a p-value greater than 0.05. Lastly, a long set of N synthetic storms characterised by rainfall-duration pairs are generated randomly by using the best copula identified.

3.4. Delineation of pluvial flood hazard maps

The series of N synthetic rainfall-duration pairs generated by using the methodology described in Section 3.3 are the Safer_RAIN input data, considering infiltration processes with the aforementioned Green-Ampt infiltration equation (Section 2.2.3). A constant initial soil water content was considered to avoid varying the Green-Ampt parameter layers in the sequential simulation with Safer_RAIN. The outputs of Safer_RAIN are processed to obtain a long set of N water depths in each cell. Then, the T-year water depth is estimated by using a frequency analysis in each cell.

Flood hazard maps are usually obtained for a set of return periods that represent the expected exceedance probability in a given year. However, the N synthetic rainfall-duration pairs represent the storms expected to exceed the threshold of 10 mm in 30 min with a mean value of λ exceedances per year (Eq. (14)). Consequently, the N water depths in each cell do not represent the annual maximum water depths expected in N years, though the water depths that are expected to exceed a threshold in N/λ years. The relationship between the return period in an annual maximum series analysis (T_a) and the return period in a POT series (T_p) is given by Eq. (17) (Stedinger et al., 1992).

$$T_p = -\frac{1}{ln\left(1-\frac{1}{T_a}\right)} \tag{17}$$

where T_p is the return period in a POT series and T_a is the return period in an AMS. Clearly, T_p will be smaller than T_a, as more than one event is expected to exceed the threshold per year in a POT series.

3.5. Comparison with the standard approach

The next step of the methodology consists of a comparison between the results of the stochastic methodology proposed in this study with the standard approach based on catchment response times used in practice. The standard approach assumes that the T-year pluvial flood in a given depression is generated by the T-year storm with a duration equal to the time of concentration of the draining catchment to such a depression.

Three depressions identified in the Safer_RAIN pre-processing phase in the Pamplona metropolitan area have been selected for the comparison: a motorway depression at Zizur Mayor and two depressions in the Echavacóiz neighbourhood and at Soto Aizoáin street at an industrial estate at Orcoyen (Fig. 5).

The time of concentration of the draining catchment to each depression is estimated by using the velocity method that estimates travel times along the hydraulically most distant flow path (NRCS, 2010). Then, the design storms estimated for a duration equal to the time of concentration are used as input data of the Safer_RAIN algorithm, comparing the outputs with the results of the stochastic methodology in a set of cells selected in each such depression.

3.6. T-year Water depth estimate uncertainty assessment

The last step of the methodology consists of quantifying the uncertainty of the T-year water depth estimates obtained with the stochastic methodology proposed in this study. In Section 3.4, T-year water depths are estimated from outputs of the Safer_RAIN algorithm by using a given set of N storm rainfall-duration pairs generated by the copula fitted to the observations (Section 3.3). Therefore, such water depth quantiles could be conditioned by the set of rainfall-duration pairs used in each case.

Therefore, the stochastic methodology has been replicated ten times, generating ten sets of N storm rainfall-duration pairs with the copula fitted to the observations. The Safer_RAIN algorithm is run by using each set of N rainfall-duration pairs as input data. For each set of N rainfall-duration pairs, T-year water depths are estimated in each cell of the Pamplona metropolitan area by using the frequency analysis described in Section 3.4.

The uncertainty analysis has been limited to the draining catchment to the Orcoyen depression delineated in Section 3.5 (Fig. 5) to reduce the

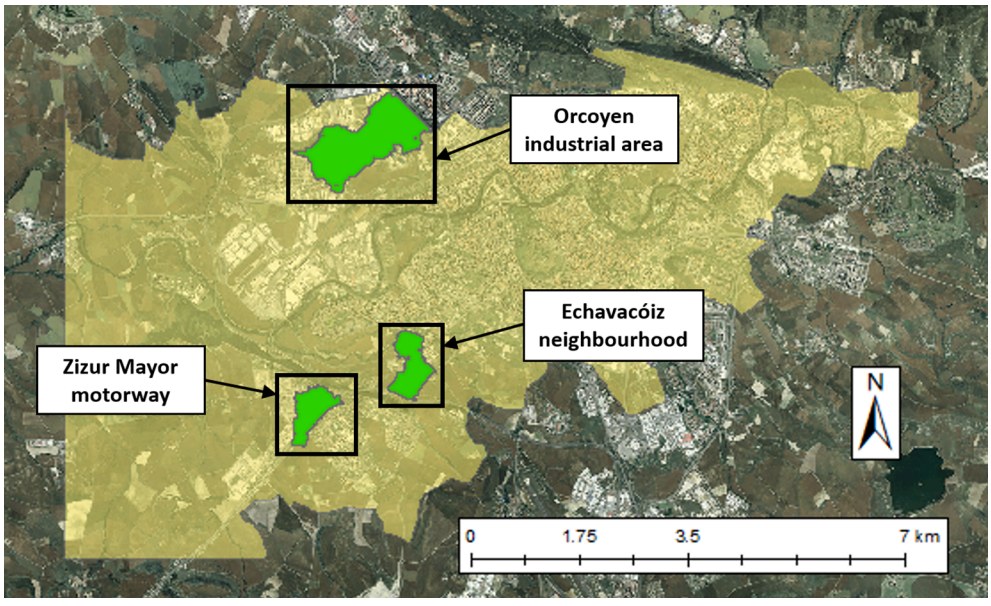

Fig. 5. Contributing catchment areas (green) to the three depressions considered for the validation between the stochastic methodology and the standard approach. Source of background layer: IGN.

computation times of the Safer_RAIN algorithm. The stochastic methodology uncertainty is assessed by analysing the dispersion of the ten *T*-year water depth estimates for each return period in five cells located in the Orcoyen depression (Fig. 12c).

4. Results

This involves six steps. First, the results of the benchmarking activities to validate the outputs of the Safer_RAIN model with the hydrodynamic simulations of IBER in four real storms are presented. Second, the application of the stochastic methodology to generate synthetic rainfall events that maintain the statistic properties of real rainfall events which exceed a given threshold is offered. Third, the results of pluvial flood hazard mapping in the Pamplona metropolitan area are shown. Fourth, the results obtained from the comparison between the stochastic methodology and the standard approach are presented. Fifth, bivariate return-period curves are estimated in a set of cells located in three depression of the Pamplona metropolitan area. Sixth, and lastly, the uncertainty in *T*-year water depth estimates is assessed in five cells located in the Orcoyen depression.

4.1. Safer_RAIN benchmarking in Pamplona

The outputs of the Safer_RAIN algorithm are compared with water depths simulated by the IBER hydrodynamic model six hours after the end of the rainfall event in the Barañáin and Zizur Mayor municipalities, considering the precipitation fields in four real storms (Table 2). The first storm of 18 September 2019 is not considered in the Barañáin municipality as it did not affect the area significantly (Fig. 3). Fig. 6 shows the outputs of the Safer_RAIN algorithm and the IBER 2D hydrodynamic model for the pluvial flood event of 20 July 2010 in the Barañáin municipality. Such a figure confirms that Safer_RAIN correctly identifies the main depressions prone to flooding in pluvial flood events. The results obtained from the other two storms in Barañáin and the four storms in Zizur Mayor are included in the supplementary material (Fig. S1–S6).

Fig. S7 and Fig. S8 show the errors in water depths between the outputs of Safer_RAIN and IBER. Most of the pixels show yellow and orange colours that point to a generally slightly lower estimate of water depths by Safer_RAIN. It can be explained by the hydrostatic assumptions of Safer_RAIN that neglects backwater dynamic curves in overland flows.

Fig. 7 shows the NSE values in Barañáin and Zizur Mayor (Eq. (12)). The highest NSE values (blue areas) are obtained in the main depressions, pointing to a good prediction of Safer_RAIN in the areas prone to pluvial flooding where water is stored and water depths are greater. On the contrary, negative values of NSE (red areas) are usually located in zones with small water depths. Fig. 8 shows the histograms of NSE in terms of the magnitude of $\overline{WD}_{IBER}$ (WD in the figure legend) in Barañáin and Zizur Mayor. In Barañáin, most of cells have high values of NSE regardless the magnitude of water depths. In addition, 50 % of cells with $\overline{WD}_{IBER}$ greater than 1 m have a NSE value greater than 0.6. In Zizur Mayor, the percentage of cells with high values of NSE increases with water depths. For small water depths with values of $\overline{WD}_{IBER}$ between 0.1 and 0.2 m, 30 % of cells have NSE values between −0.6 and −1 and only 10 % between 0.6 and 1. However, for the greatest water depths with $\overline{WD}_{IBER}$ values greater than 1 m, almost 80 % of cells have NSE values greater than 0.6. Consequently, Safer_RAIN supplies good predictions in depressions where greater water depths are expected, though it supplies worse predictions in zones with small water depths.

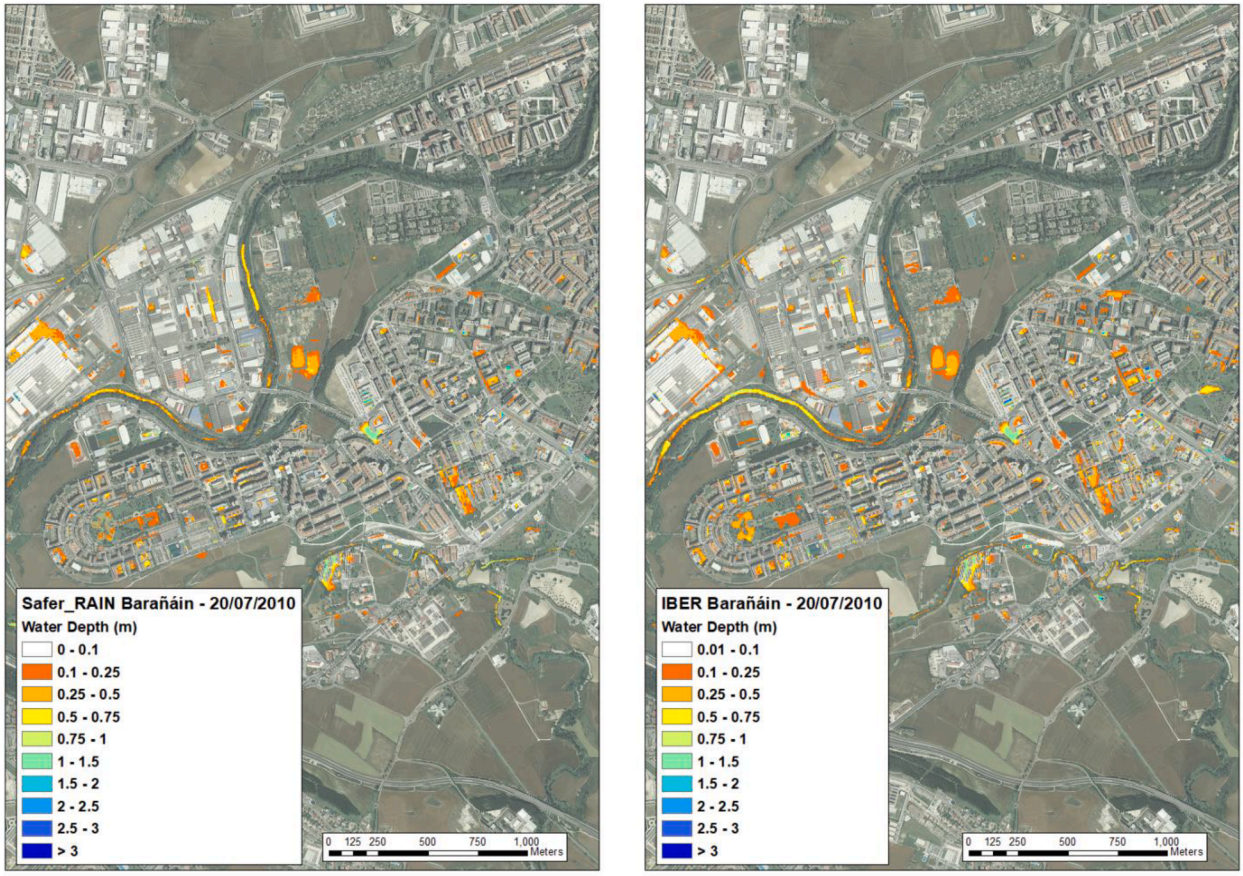

Fig. 6. Comparison between hydrostatic simulations with Safer_RAIN (left column) and hydrodynamic simulations with IBER (right column) in the Barañáin municipality for the pluvial flood event of 20 July 2010. Source of background layer: IGN.

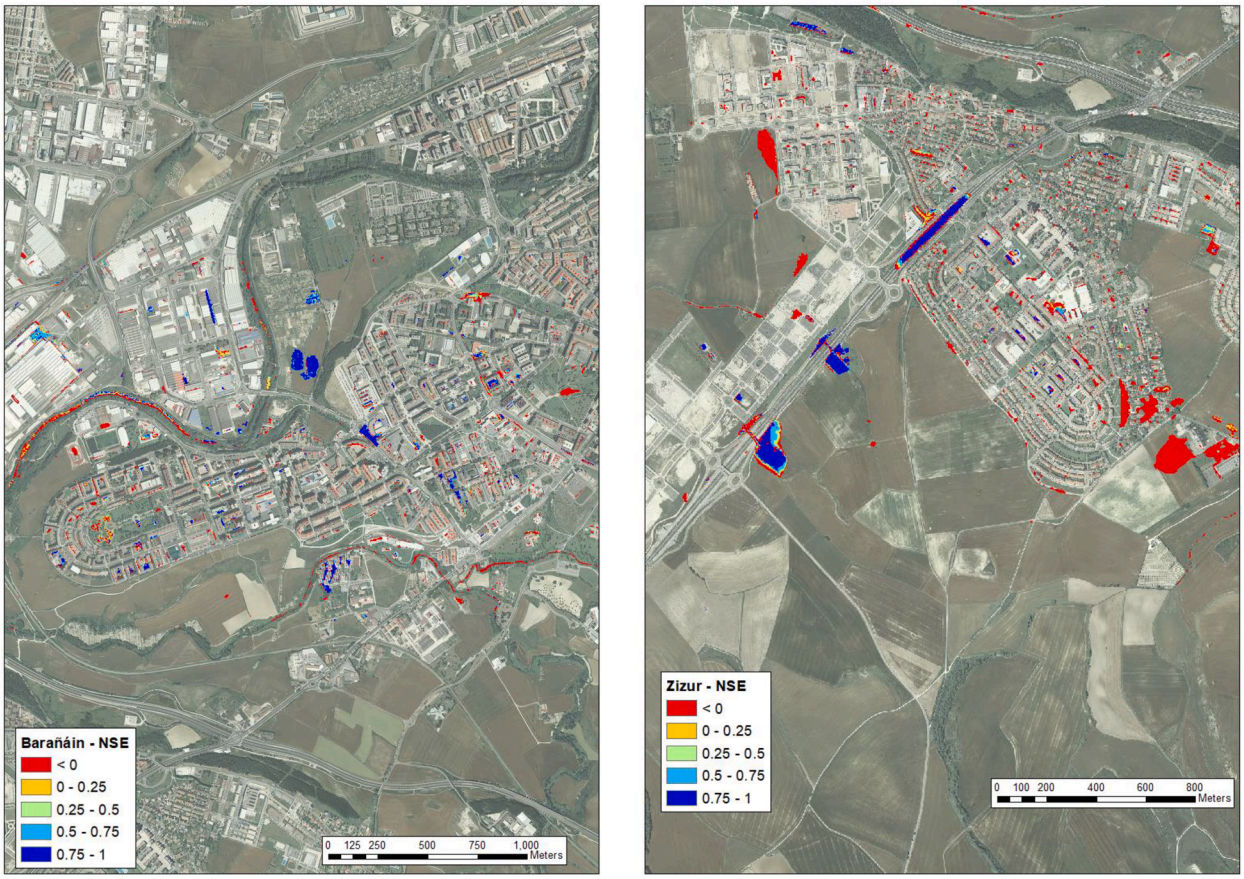

Fig. 7. NSE values between Safer_RAIN and hydrodynamic simulations with IBER calculated for the four pluvial flood events: a) Barañáin; b) Zizur Mayor. Source of background layer: IGN.

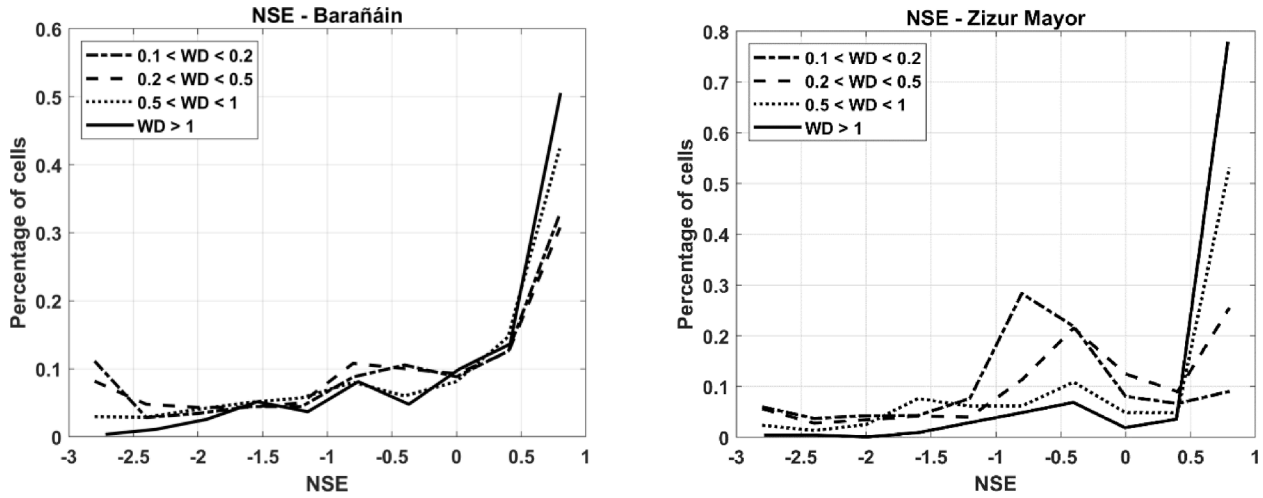

Fig. 8. Histogram of NSE values between Safer_RAIN and hydrodynamic simulations with IBER calculated for the four pluvial flood events in terms of water depths: a) Barañáin; b) Zizur Mayor. Source of background layer: IGN.

The bias, RMSE, CSI, R_{TP}, R_{TN}, ACC, and MCC objective functions are used to quantify the differences in water depths between IBER and Safer_RAIN outputs (Table 3).

In Barañáin, the bias is between −2 and 4 cm that points to small errors in water depths. Such values close to zero mean that Safer_RAIN compensates positive and negative errors and does not tend either to overestimate or underestimate water depths at Barañáin. The RMSE values are greater, between 19 and 25 cm, as they do not account for compensation between positive and negative errors. In terms of flood extents, the CSI values are 0.42 and 0.45 for the 2010 and 2020 events, respectively, and close to 0.3 for the second storm of 2019, indicating that Safer_RAIN represents correctly the 30–40 % of the flood extent simulated by IBER. R_{TP} is 0.5 for the events of 2010 and 2020 and 0.38 for the second storm of 2019, meaning that Safer_RAIN correctly simulates 50 % and 38 %, respectively, of the flooded cells simulated by IBER. These results may show good agreement between the models,

Table 3
Results obtained from the comparison between the Safer_RAIN outputs and the IBER simulations six hours after the end of the storm.

Location	Pluvial flood event	Bias (m)	RMSE (m)	CSI (-)	R_{TP} (-)	R_{TN} (-)	ACC (-)	MCC (-)
Barañáin	20 July 2010	−0.024	0.245	0.453	0.505	0.993	0.967	0.626
	18 September 2019 – Storm 1	–	–	–	–	–	–	–
	18 September 2019 – Storm 2	0.039	0.193	0.294	0.384	0.994	0.982	0.454
	25 April 2020	0.032	0.192	0.421	0.507	0.992	0.975	0.589
Zizur Mayor	20 July 2010	−0.218	0.480	0.309	0.321	0.998	0.970	0.524
	18 September 2019 – Storm 1	0.158	0.262	0.238	0.456	0.997	0.995	0.386
	18 September 2019 – Storm 2	0.026	0.278	0.376	0.425	0.998	0.991	0.567
	25 April 2020	−0.004	0.285	0.343	0.366	0.999	0.985	0.550

accounting for the limitations of the hydrostatic assumptions of Safer_RAIN regarding the hydrodynamic simulations of IBER. R_{TN} and ACC are close to one in the three events, proving that the percentage of agreements in cells is high, either flooded or non-flooded, and in line with that observed in Samela et al (2020). Lastly, MCC values are between 0.45 and 0.63, meaning that Safer_RAIN provides a good prediction of the IBER simulations.

At Zizur Mayor, the bias is between −21 and 16 cm with a value close to zero in the second storm of 18 September 2019. The RMSE values are between 0.26 and 0.28 in the 18 September 2019 flood event. The event of 20 July 2020 provides a RMSE value of 0.48. Therefore, at Zizur Mayor, Safer_RAIN tends to underestimate water depths, with greater RMSE values for the highest rainfall magnitude. CSI values are between 0.24 and 0.38 which indicates that 24–38 % of the flood extents simulated by IBER are predicted correctly by Safer_RAIN. R_{TP} values are between 0.32 and 0.46, revealing agreement of 32–46 % of Safer_RAIN with the flooded cells of IBER. As stated above, these results provide agreement of Safer_RAIN and account for hydrostatic limitations. R_{TN} and ACC are close to one in the four flood events considered at Zizur Mayor. Therefore, the percentage of agreements in cells, either flooded or non-flooded, is also high. MCC values are equal to 0.52 and 0.57 in the 20 July 2010 and, respectively, the second storm of 18 September 2019 flood events. The MCC values are smaller for the first storm of 18 September 2019 with a value close to 0.4. Therefore, it is clear that Safer_RAIN provides a good prediction of the IBER simulations in terms of flood extents, mainly in the flood events of 20 July 2010 and the second storm of 18 September 2019.

Comparing the results in Pamplona (Spain) with those obtained in Rimini (Italy) (Samela et al., 2020), sensitivity (R_{TP}) is up to 71 % in Rimini and up to 50 % in Pamplona. However, at Pamplona specificity (R_{TN}) is slightly greater with values of 99 % in all the cases. Accuracy values obtained from ACC are similar. Samela et al. (2020) found that while sensitivity increases with storm precipitation, accuracy decreases slightly. The return periods of the four real storms considered in the benchmark analysis in Pamplona are below 20 years. Therefore, the smaller sensitivity values may be explained by smaller precipitations in the storms considered in Pamplona.

In summary, small CSI values indicates that flood extents predicted by Safer_RAIN are usually smaller than expected. However, high NSE values for the greatest water depths point to a good prediction in the main depressions with the highest water depths and the greatest flood hazards. Therefore, the Safer_RAIN tool offers adequate results at Barañáin and Zizur Mayor, considering the hydrostatic assumptions of Safer_RAIN regarding the hydrodynamic behaviour of IBER and the high reduction of computation times from hours to around one minute.

4.2. Stochastic generation of rainfall events

The first step in stochastic generation of rainfall events consists of the extraction of real storms that exceed the threshold of 10 mm in 30 min. Cumulative precipitation in two consecutive time steps is considered in the 15–min rainfall time series and in three consecutive time steps in the 10-min rainfall time series (Fig. S9). In a given storm, several consecutive time steps could have a cumulative precipitation over the threshold. Therefore, the beginning and ending time steps of storms were identified.

Table 4 shows that the four rain-gauging stations have similar values of λ, indicating an analogous rainfall behaviour with a similar probability of storm arrival exceeding the threshold of 10 mm in 30 min at the four stations. Therefore, the storms can be aggregated in a unique series of 138 rainfall events, as rainfall-gauging sites are close enough to have a similar rainfall behaviour, though far enough to record different storms in pluvial flood events that are characterised by precipitations with high spatial variability. The mean annual number of exceedances over the threshold for the aggregated data is calculated as the weighted mean of λ by the record length at each station, obtaining a value of 2.03 exceedances per year.

The marginal distributions of storm rainfall depth and duration are obtained by using a GP distribution with the L-moments method (Fig. 9). The rainfall depth frequency curve has a lower bound of 10 mm that corresponds to the POT threshold, guaranteeing that the synthetic rainfall events generated by the copula-based approach will have a precipitation equal or higher to such a threshold and avoiding the generation of events with smaller precipitation that could not drive pluvial floods. The duration frequency curve has a lower bound of 30 min, which also agrees with the POT threshold, and an upper bound close to 3.5 h. Therefore, the synthetic rainfall events will have durations between 0.5 and 3.5 h, avoiding the generation of excessively short or long storms that could not drive pluvial floods.

The Clayton, Frank, and Gumbel family copulas were fitted to the aggregated 138 precipitation-duration pairs (Fig. 10). The S_n goodness-of-fit test and p-value were obtained by using 10 000 parametric bootstrap samples for each copula family (Table 5). The results show that the Clayton and Frank copulas have a p-value lower than 0.05, indicating that they are unable to characterise the dependence relationship between precipitation and duration pairs. As only the Gumbel copula obtained a p-value higher than 0.05, it cannot be rejected. In addition, the Gumbel copula also leads to the lowest value of the S_n statistic. Consequently, the Gumbel copula is the most appropriate when characterising the dependence structure of the 138 precipitation-duration pairs of real rainfall events that can drive pluvial floods in the Pamplona metropolitan area.

4.3. Pluvial flood hazard maps in Pamplona

A set of 10 000 random precipitation-duration pairs was generated with the Gumbel copula fitted in Section 4.2, obtaining short durations

Table 4
Main characteristics of POT series that exceed a threshold of 10 mm in 30 min in the four rain-gauging stations considered in the study: t is the period length (years), m is the number of exceedances over the threshold in the period t, and λ is the mean annual number of exceedances over the threshold.

Rainfall-gauging station	t (years)	m	λ
P1	23	48	2.09
P2	19	40	2.11
P3	10	24	2.4
P4	16	26	1.63

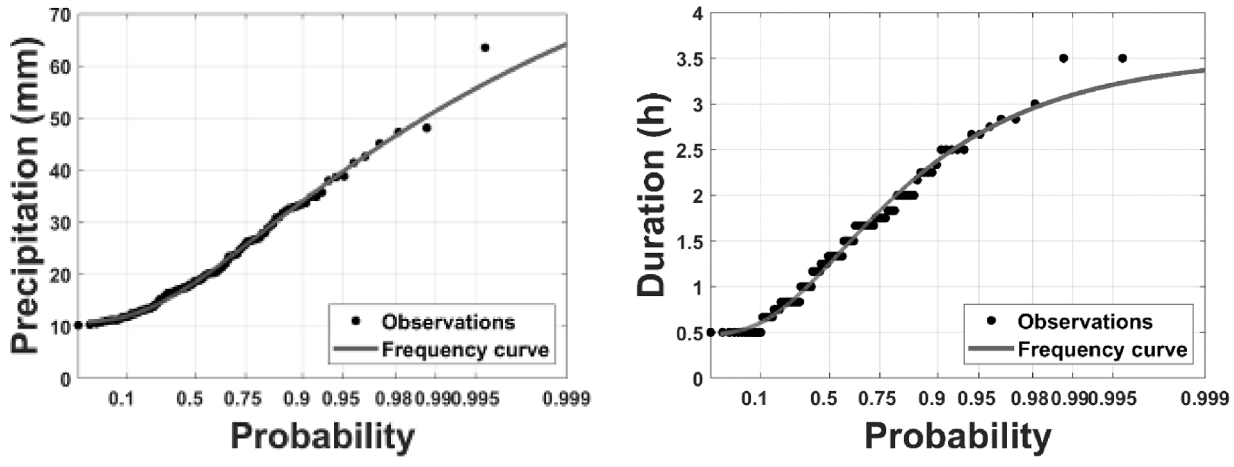

Fig. 9. GP distribution functions fitted to the rainfall depth (left) and duration (right) of the 138 real storms that exceed the threshold of 10 mm in 30 min at the four gauging sites considered in the study.

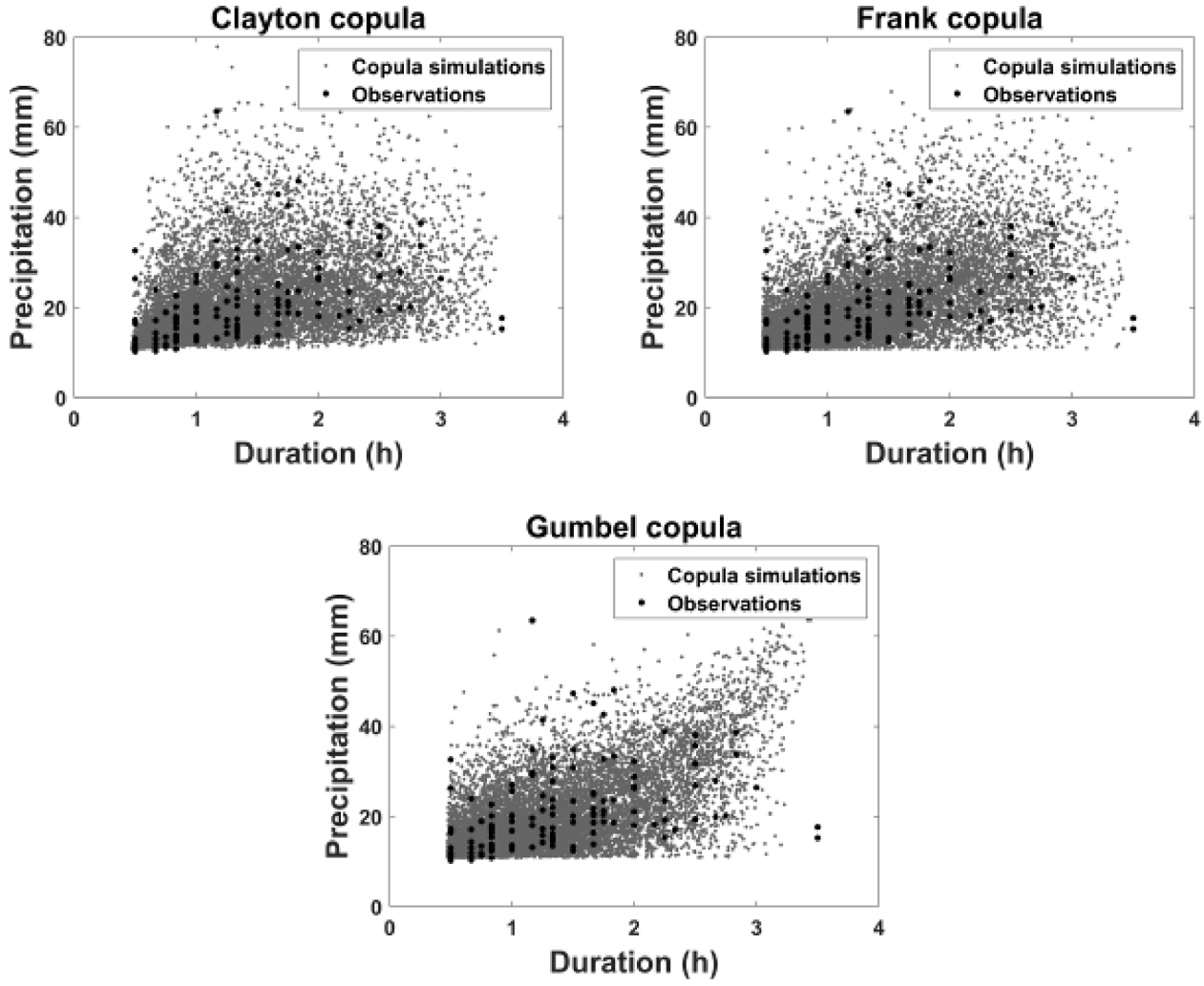

Fig. 10. Comparison between the precipitation-duration pairs of the 138 real rainfall events extracted in Pamplona (black points) and 10 000 random simulations generated by the fitted copula (dark grey points): a) Clayton copula, b) Frank copula; c) Gumbel copula.

between 0.5 and 3.5 h and rainfall depths equal or greater than 10 mm required to generate pluvial floods in Pamplona (Fig. 10c). The Safer_RAIN algorithm was run with the 10 000 synthetic storms and considered infiltration processes with the Green-Ampt model. The Safer_RAIN algorithm is embedded in the SaferPlaces platform in Pamplona (https://platform.saferplaces.co). However, a Jupiter Notebook script in Google Colaboratory was used to run such a long number of simulations iteratively. The Safer_RAIN pre-process was run once in the Pamplona

Table 5
Estimated value of the copula parameter (θ_n), Cramér-von Mises goodness-of-fit test (S_n), and p-value with 10 000 parametric bootstrap samples for the Clayton, Frank, and Gumbel copulas.

Copula	Θ_n	S_n	p-value
Clayton	1.202	0.9995	0.023
Frank	4.054	0.993	0.032
Gumbel	1.486	0.632	0.089

metropolitan area for 121.40 s. The flooding phases (i.e. the filling and spilling processes) were simulated in around 45 s for each event, supplying water depths in each cell.

In a given cell, the water-depth distribution can include several zeros that represent the storms that do not generate enough water accumulation in the depression to flood the cell. In addition, it can show an upper bound that represents 100 % filling water depth in the depression. Therefore, no distribution function could fit such data adequately. In each cell, T-year water depths were estimated empirically from the sorted series of 10 000 water depths, by using the Weibull plotting position formula and considering the return periods in a POT analysis (T_p) (Eq. (17)). Seven return periods are considered: two, five, 10, 25, 50, 100 and 500 years. Fig. 11 shows the pluvial flood hazard maps for the two-, 10-, 100- and 500-year return periods. The hazard maps for other three return periods (five, 25 and 50 years) are included in the supplementary material (Fig. S10-S12).

The main pluvial flood hotspots in Pamplona could be identified from such maps (Fig. 11b): (i) the motorway depression at Zizur Mayor; (ii) the Soto Aizoáin street at the industrial estate of Orcoyen, driven by a building with three industrial units that obstructs a former stream; (iii) Echavacóiz neighbourhood, driven by a levee to protect the area from River Elorz fluvial floods; (iv) depression at the Miluze and Ermitagaña crossroads; (v) railway underpass at San Jorge; (vi) a depression at the Sadar street; (vii) a depression between Txantrea and Burlada, and (viii) a depression at the Burlada sports centre, driven by a levee to protect the area from River Arga fluvial floods.

4.4. Comparison with the standard approach

The results of the stochastic methodology with Safer_RAIN are compared with the standard approach that considers the T-year storm precipitation for a duration equal to the draining catchment response time. A time of concentration of 25 min was estimated at the motorway depression at Zizur Mayor, 50 min at the Echavacóiz neighbourhood, and 75 min at the Orcoyen industrial area, by using the velocity method that estimates travel times along the hydraulically most distant flow path (NRCS, 2010). Table 6 includes the T-year storm precipitations considered in each depression. A set of cells have been selected in each zone to compare the distribution of 10 000 water depths obtained by using the stochastic methodology with the standard approach results (Fig. 12). The cells for the comparison have been selected, scattered in main depressions where water is stored to characterise adequately the filling processes. In this case, 10 return periods are used for the comparison: two, five, 10, 20, 25, 30, 50, 100, 200 and 500 years.

Fig. 13 shows the results for the two cells considered in the motorway depression at Zizur Mayor. The distribution of water depths obtained with the stochastic methodology adequately fits the water depths obtained by the standard approach.

Both approaches agree about when the depression begins to fill in Cell 2 at a return period of below two years. However, in Cell 1 the filling process begins for the 10-year return period for the stochastic methodology and between two and five years for the standard approach. In the filling process, water depths are similar in each approach, though water depths are greater for the standard approach for low return periods. The differences in water depths between the approaches are reduced as the return period increases in Cell 1. In Cell 2, water depths for the

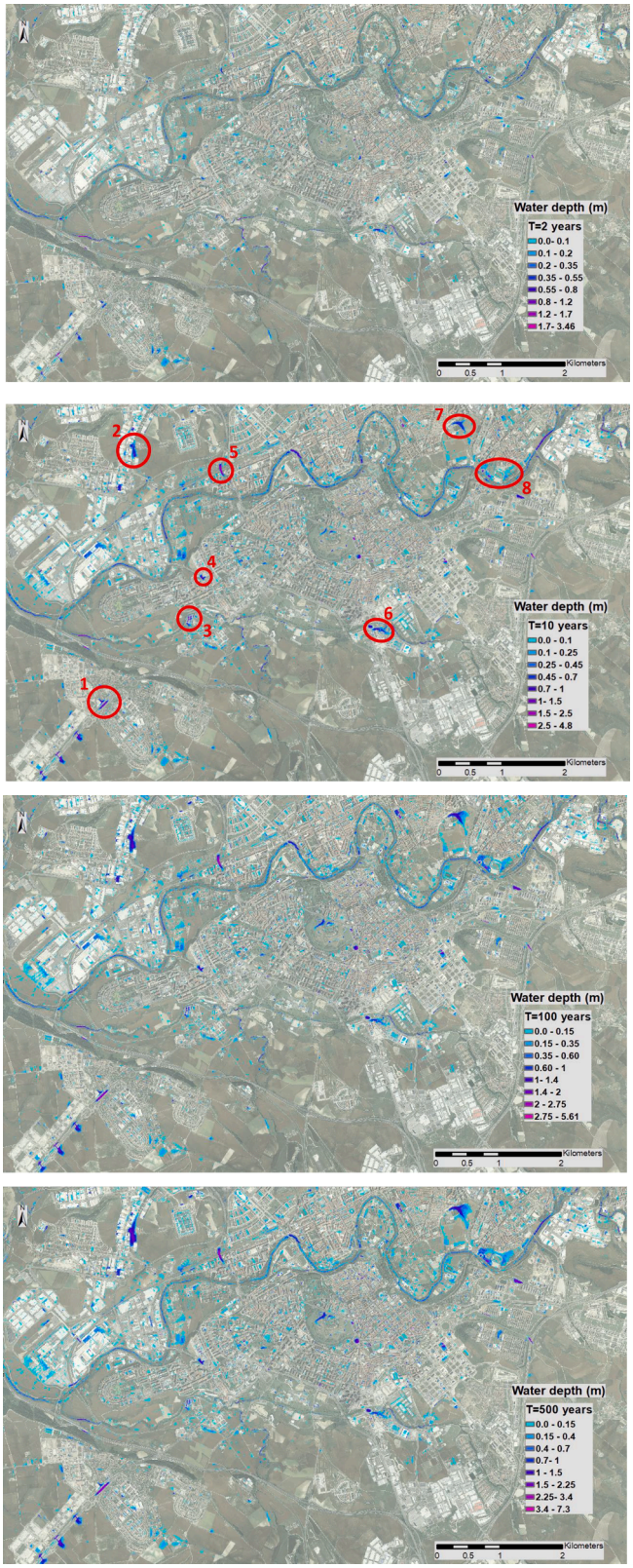

Fig. 11. Pluvial flood hazard maps developed with the Safer_RAIN stochastic methodology for selected return periods in years: a) two; b) 10; c) 100; and d) 500. Source of background layer: IGN.

Table 6
T-year storm precipitations considered in the three depressions selected to compare the stochastic methodology with the standard approach.

Return period (years)	Precipitation (mm)		
	Motorway depression at Zizur Mayor (D = 25 min)	Echavacóiz neighbourhood (D = 50 min)	Orcoyen industrial area (D = 75 min)
2	13.92	17.22	18.79
5	20.42	24.16	25.90
10	24.73	28.76	30.61
20	28.86	33.17	35.13
25	30.17	34.56	36.56
30	31.23	35.70	37.72
50	34.21	38.87	40.97
100	38.21	43.15	45.35
200	42.20	47.41	49.72
500	47.47	53.04	55.48

stochastic methodology are slightly greater for the highest return periods.

In the Echavacóiz neighbourhood, both methods provide agreement regarding the beginning of the filling process of between two and five years in Cell 1 and five and ten years in Cell 3 (Fig. 14). In Cell 2, the filling process begins for the two-year return period for the standard approach and between two and five years for the stochastic methodology. In this case, the stochastic methodology simulates the filling process faster than the standard approach in the three cells, as the return period for the 100 % depression filling is smaller for the stochastic methodology. However, distributions show a similar shape for each methodology and water depth differences for given return periods are small in the range of 10 cm.

In the Orcoyen commercial area (Fig. 15), water-depth distributions show similar shapes and point to an adequate simulation of the depression filling processes in each case, though the standard approach estimates slightly greater water depths. The filling process in the depression begins at lower return periods in the standard approach. The greatest differences between water depths for given return periods are for the lowest return periods, with the differences becoming smaller for high return periods.

4.5. *Bivariate pluvial flood return periods*

In addition, the stochastic methodology can supply information about the relationship between the variables that characterise storms and pluvial flood water depths in a given depression (Mediero et al., 2010). Specifically, the set of storms that generate water depths higher than the *T*-year water depths estimated empirically in Section 4.3 can be identified in a given depression, obtaining the bivariate return-period curves of pluvial floods in the three depressions selected as case studies in Section 3.5. Fig. 16 shows that the *T*-year water depth in a given depression is not driven by a unique storm, such as the design storm, rather than by a set of storms with different combinations of precipitation and storm duration. For example, the five-year water depth in Cell 5 of the Orcoyen depression (boundary between green and blue colours in Fig. 16c) is generated by a set of storms: 16.6 mm in 30 min, 23.3 mm in one hour, 27.5 mm in 1.5 h and 30.5 mm in two hours, among others. Consequently, the bivariate return-period curve for a given return period *T* identifies the possible combinations of precipitation and storm duration that generate the *T*-year pluvial flood.

Bivariate return-period curves show that precipitation increases with storm duration for a given return period, though the relationship is not linear. Such an increasing relationship is related to both the mean rainfall intensity and precipitation losses generated by infiltration processes in a given storm. For a given bivariate return-period curve, while the precipitation increases with storm duration, the mean rainfall intensity decreases with storm duration. This indicates that a shorter storm with a higher mean rainfall intensity can generate the same water depth than a longer storm with a smaller mean rainfall intensity.

In addition, rainfall water volumes increase with storm precipitation, with greater water depths being expected. However, for a given storm

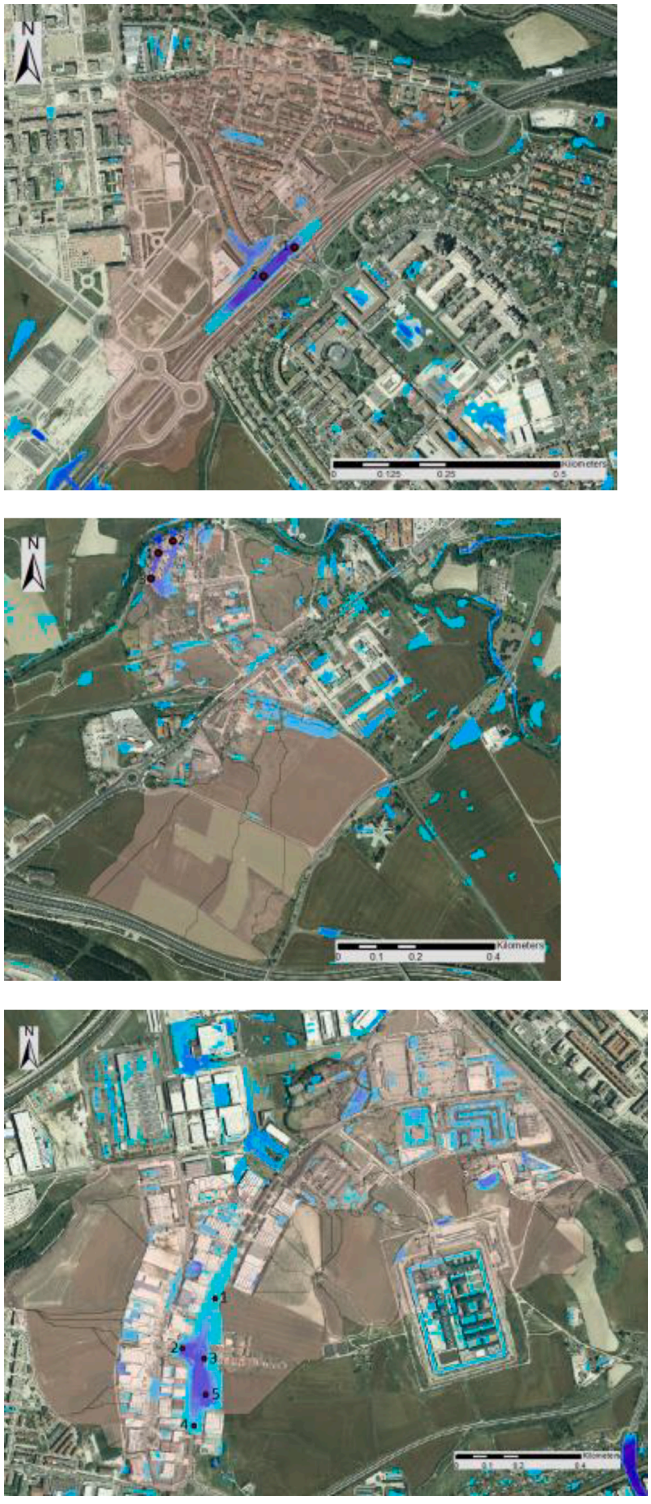

Fig. 12. Cells selected for the comparison between the stochastic methodology and the standard approach (black dots). Blue areas represent the depressions. Shaded areas represent the draining catchments. a) two points selected at the motorway depression at Zizur Mayor; b) three points selected at the Echavacóiz neighbourhood, and c) five points selected at the Orcoyen industrial area. Source of background layer: IGN.

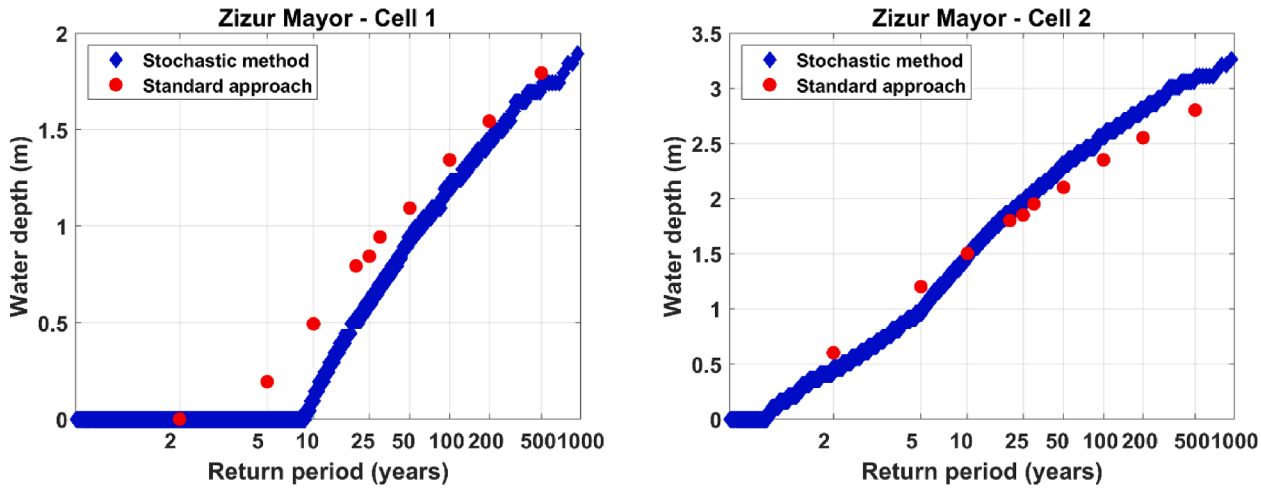

Fig. 13. Comparison between the distribution of 10 000 water depths obtained by using the stochastic methodology (blue diamonds) with the design water depths estimated by using the standard approach (red dots) in the motorway depression at Zizur Mayor.

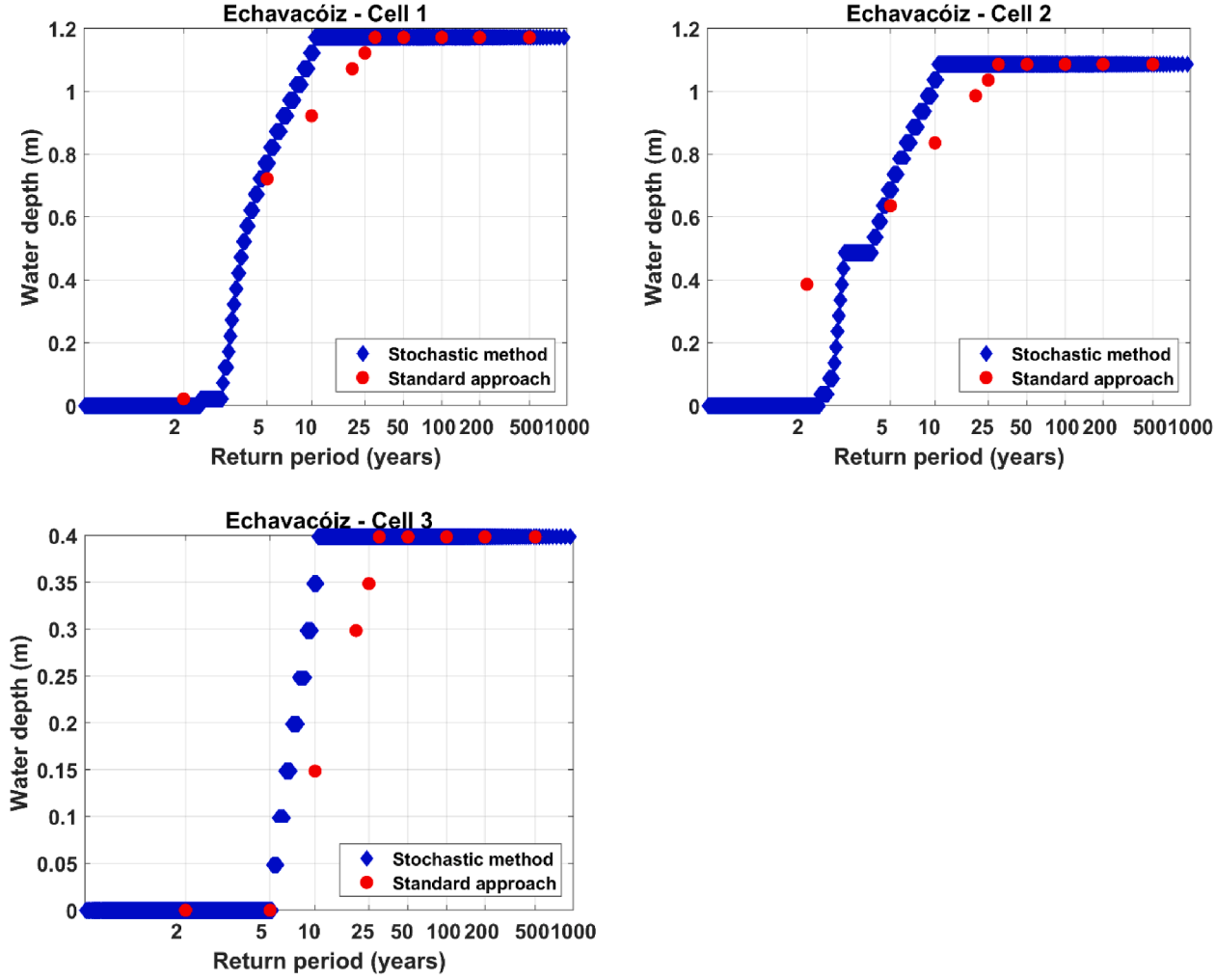

Fig. 14. Comparison between the distribution of 10 000 water depths obtained by using the stochastic methodology (blue diamonds) with the design water depths estimated by using the standard approach (red dots) at the Echavacóiz neighbourhood.

precipitation, water runoff volume decreases as storm duration increases because infiltration processes give place to greater rainfall losses. Higher rainfall losses are generated in rural catchments with high infiltration rates. Nevertheless, smaller rainfall losses are expected in urban catchments where soils are mostly sealed and infiltration rates are lower. Therefore, bivariate return-period curves will have steeper slopes in rural catchments than in urban catchments. Furthermore, return-period curves could even be horizontal in a catchment with soils completely

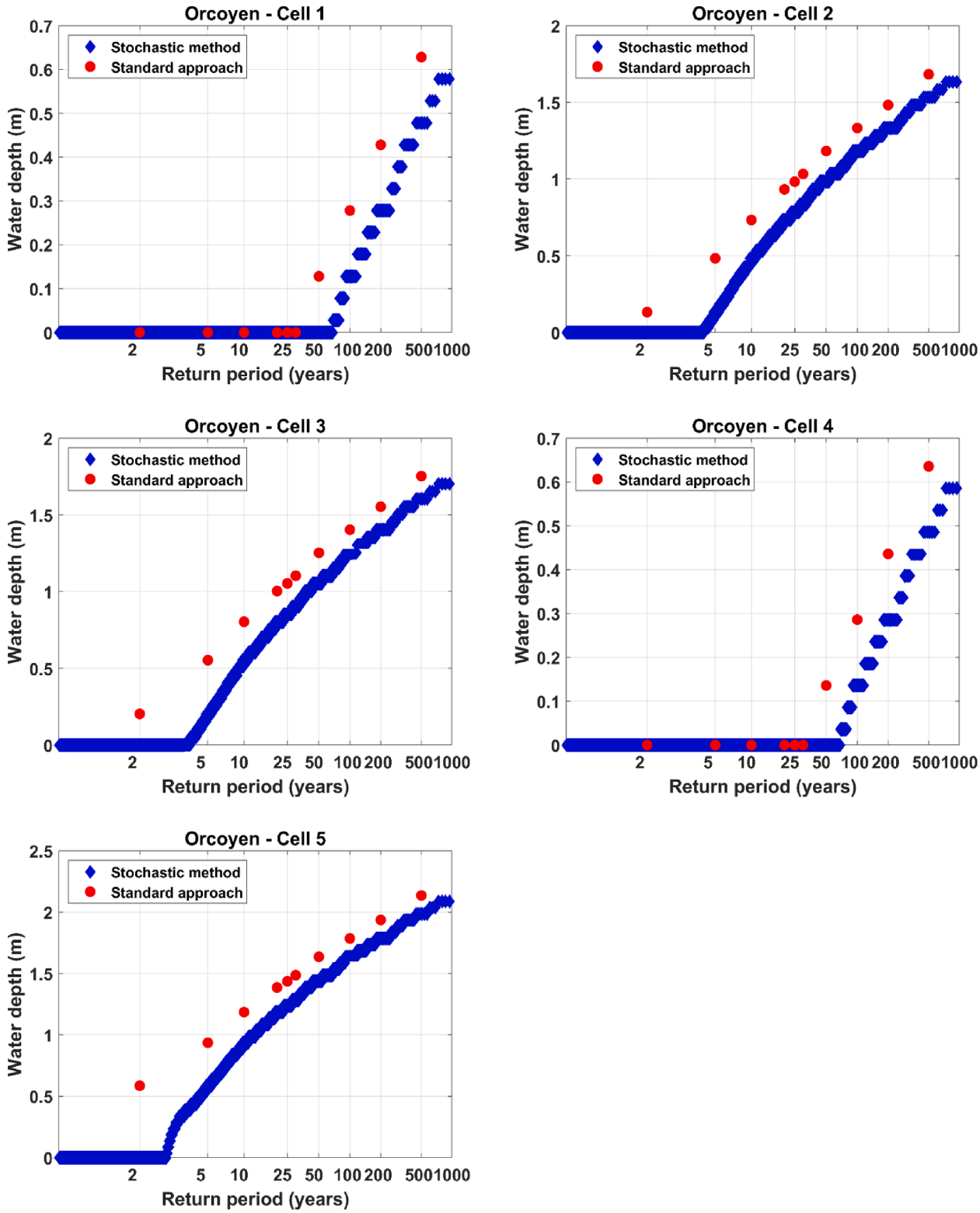

Fig. 15. Comparison between the distribution of 10 000 water depths obtained by using the stochastic methodology (blue diamonds) with the design water depths estimated by using the standard approach (red dots) at the Orcoyen industrial area.

sealed where no rainfall losses will be generated.

In the three depressions selected in Section 3.5, the draining catchment at the Orcoyen depression is mostly rural, the catchment in Echavacóiz is a mixture of rural and urban areas, and the Zizur Mayor motorway depression has a draining catchment that is mostly urban. Therefore, the Zizur Mayor depression will have the mildest bivariate return-period curve slope, as its draining catchment is mostly urban and rainfall losses are smaller, smoothing the increasing relationship between precipitation and storm duration for a given bivariate return-period curve. However, the Orcoyen depression will show the steepest bivariate return-period curve, as its mostly rural draining catchment increases rainfall losses.

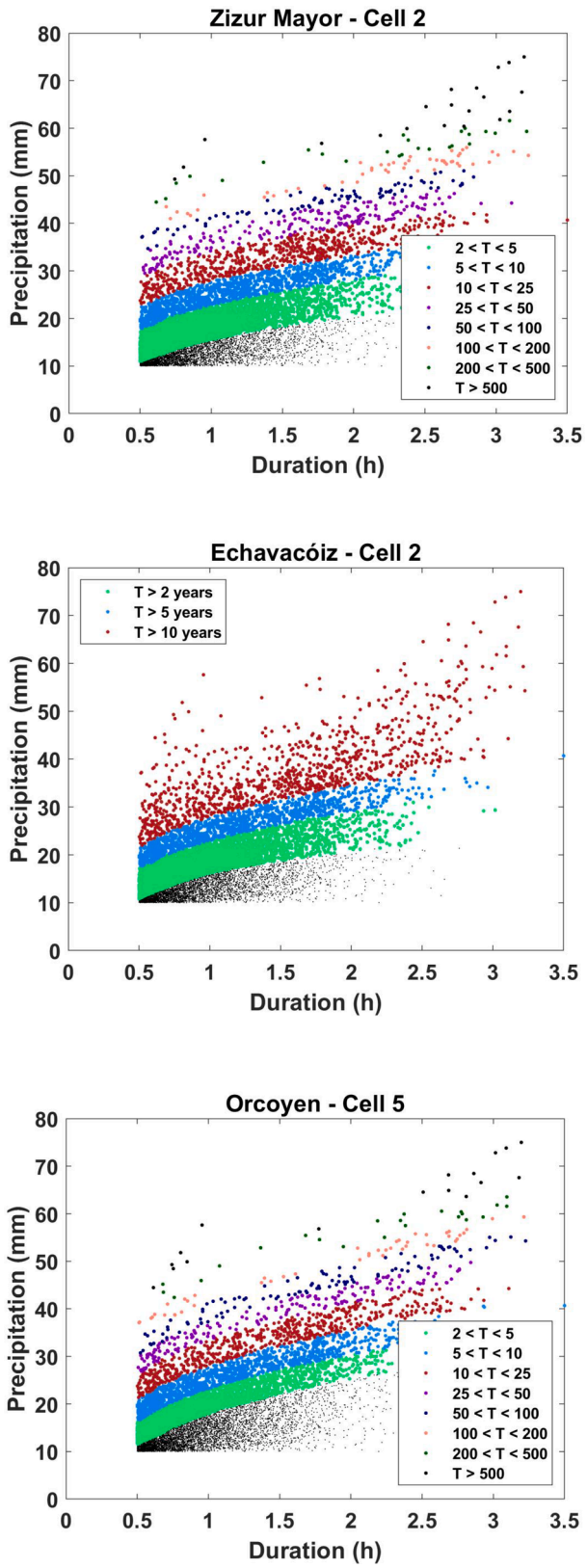

Fig. 16. Bivariate return periods (*T*) of pluvial floods in: a) Cell 2 in the Zizur Mayor motorway depression; b) Cell 2 in the depression at the Echavacóiz neighbourhood; and c) Cell 5 in the depression at the Orcoyen commercial area.

4.6. Uncertainty in T-year water depth estimates

Finally, the uncertainty in *T*-year water depth estimates is assessed. Ten sets of 10 000 storm rainfall-duration pairs are generated with the Gumbel copula fitted to the observations in Section 4.2. The Safer_RAIN algorithm is run with the ten sets of rainfall-duration pairs in the draining catchment to the Orcoyen depression (Fig. 5). Five cells are selected for assessing the uncertainty of *T*-year water depth estimates (Fig. 12c), by plotting the dispersion of the ten *T*-year water depth estimates in each cell by using boxplots (Fig. 17).

Fig. 17 shows that uncertainty increases with decreasing water depths. Boxplots are greater in Cells 1 and 4, where water depths are smaller. In addition, uncertainty increases with the return period. In Cells 2, 3 and 5, the greatest uncertainties are found for the highest return periods. Furthermore, in Cells 2, 3 and 5, high uncertainties are also found for the lowest return periods with smaller water depths. This agrees with the findings of the benchmarking activities (Section 4.1), where higher errors in the Safer_RAIN algorithm outputs were found when water depths are small.

Therefore, the most reliable estimates are found for return periods between 10 and 100 years, where almost all the ten *T*-year water depth estimates agree. In addition, for high return periods, the uncertainty increases for small water depths. Therefore, the stochastic methodology supplies more reliable results in the lowest cells of the main depressions where greater water depths are expected.

5. Discussion

It can be argued that the standard approach used for pluvial flood hazard mapping in practice and based on design storms has certain drawbacks. One could be that design storms may not be feasible when considering the real storms that can arrive at the area studied. Another would be that such an approach assumes that the *T*-year storm generates the *T*-year pluvial flood event. And lastly, another would be that empirical formulae used to estimate catchment response times and durations of design storms present significant uncertainties when in practice.

The stochastic methodology proposed in this study considers the return-period concept as an exceeding water depth threshold identified from a large set of 10 000 storms with frequencies, rainfall depths and durations similar to the observations at rain-gauging stations. Therefore, such a methodology improves the standard approach, as it estimates *T*-year water depths regardless of catchment response times (avoiding the uncertainties by using empirical formulae) and design storms that could not be realistic. In addition, the stochastic methodology shows that the *T*-year water depth in a given depression can be generated by a set of storms with varying combinations of storm precipitation and duration, instead of by a single design storm. Consequently, the stochastic methodology can be considered sounder that the standard approach. Moreover, the stochastic methodology can easily be applied to multi-depression urban areas, as it does not need to estimate a design hyetograph in each depression in terms of catchment response times. However, a drawback of the proposed methodology could be the need to repeat the simulations when a mitigation measure is applied, changing flood hazards. Nevertheless, the DTM can be clipped focusing in the area where flood hazards change with the new mitigation measure, reducing the computation time of the new simulations considerably.

The benchmarking results between the Safer_RAIN algorithm outputs and the IBER 2D hydrodynamic simulations show that Safer_RAIN supplies adequate results in terms of water depths, considering its hydrostatic assumptions. Safer_RAIN supplies better predictions of water depths in depressions prone to pluvial flooding where the greatest water depths are expected, in terms of both water depth magnitude and uncertainty. However, Safer_RAIN shows some limitations to reproduce flood hazards in zones where small water depths are expected. Consequently, *T*-year water depth estimates in lower points of the main

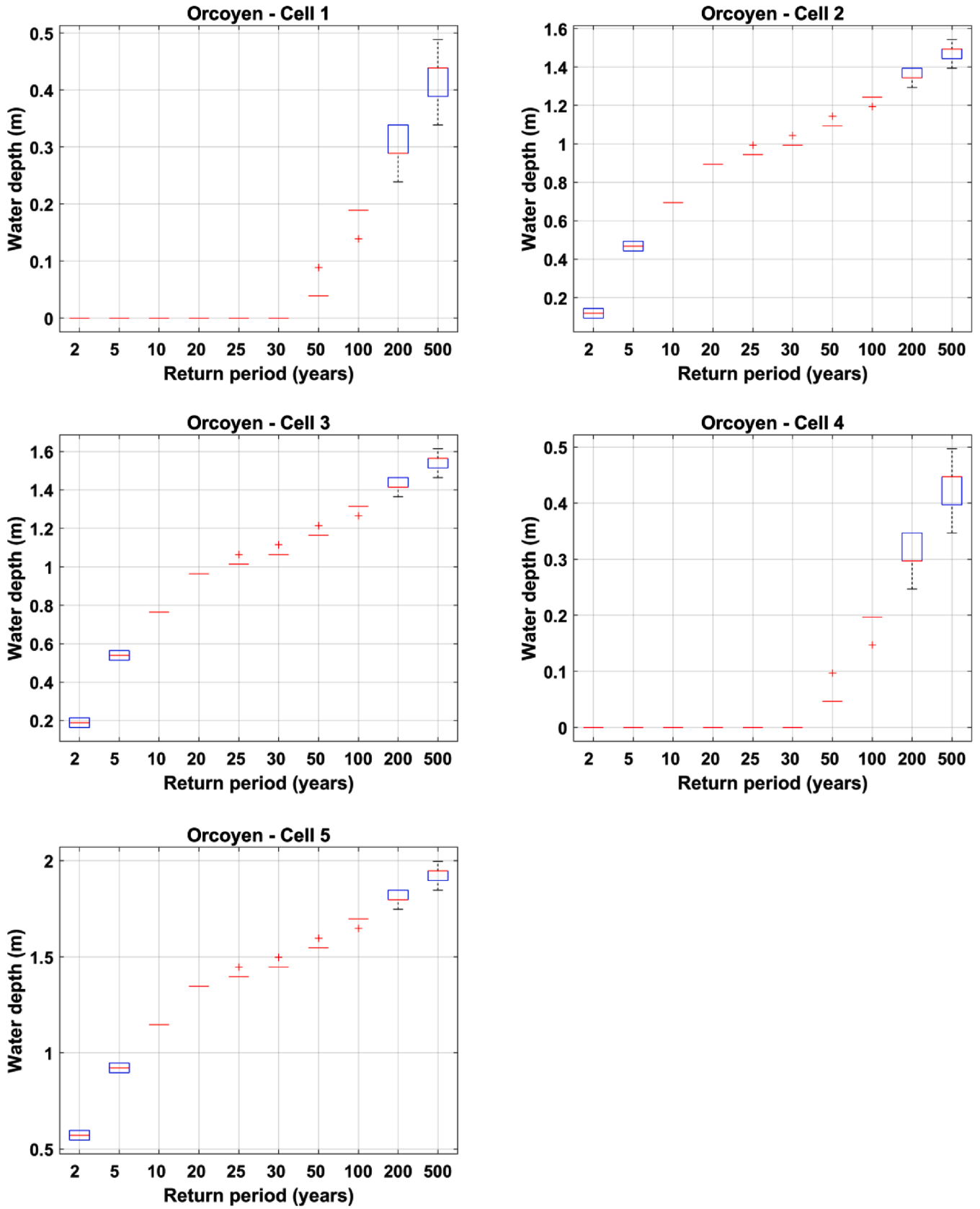

Fig. 17. Uncertainty in *T*-year water depths obtained by using the stochastic methodology. Red lines represent the median. Blue boxes represent 25th and 75th percentiles. Red crosses represent outliers.

depression are more reliable than *T*-year estimates in areas with small water depths, where such estimates should be taken with caution.

In addition, the exploratory analysis presented in this study has considered some simplifying assumptions. The first is that synthetic uniform spatial rainfall events have been considered, though the Safer_RAIN tool can consider precipitation fields with heterogeneous spatial distribution. Such a simplification avoids the complexity and computation times required for calibrating a spatially distributed rainfall generator and for simulating Safer_RAIN with precipitation fields for such a long set of storms. The second is that a constant initial soil water content in the Green-Ampt model has been considered and the urban drainage system in the Pamplona metropolitan area could not be considered, as the current version of the SaferPlaces platform does not include such functionalities yet. Lastly, the main limitation of the stochastic methodology proposed arises from the hydrostatic behaviour of the Safer_RAIN algorithm that cannot consider overland flow dynamics. However, the reduction in computation times obtained from such an assumption compared with 2D hydrodynamic models is from several hours to around one minute, allowing pluvial flood hazard maps at multi-depression cities or municipalities at spatial scales to be generated in reasonable times. Such a stochastic approach would be unaffordable with 2D hydrodynamic models. Moreover, not only *T*-year water depths are obtained in each cell but also the complete probability distribution of water depths and bivariate return-period curves in terms of precipitation and storm duration.

6. Conclusions

A stochastic methodology to delineate pluvial flood hazard maps in urban areas by using the fast-processing and DEM-based Safer_RAIN algorithm is presented. The methodology was applied to the metropolitan area of Pamplona in Spain (68.26 km^2). The Safer_RAIN algorithm was benchmarked with the IBER 2D hydrodynamic model at the Barañáin and Zizur Mayor municipalities, considering 10-min precipitation QPE fields for four real storms that generated pluvial floods in the last years. The benchmarking results showed that the Safer_RAIN algorithm offers adequate results in terms of water depths considering its hydrostatic simplifications. In addition, Safer_RAIN offers better predictions in depressions where greater water depths are expected than in flatter areas with smaller water depths.

A set of 138 real storms in which each one exceeds a threshold of 10 mm in 30 min was identified from the observations at four rainfall-gauging stations. The Gumbel copula was selected as the most suitable to represent the dependence between the 138 real storm precipitation-duration pairs. A large set of 10 000 synthetic storms with similar statistical characteristics to the real storms was generated randomly and used as input data in the Safer_RAIN algorithm, considering infiltration processes with the Green-Ampt model. The Safer_RAIN pre-process was run once in 121.40 s and the flooding phase was simulated in around 45 s for each event. Therefore, the computation time was reduced from some hours to around one minute for each event, regarding 2D hydrodynamic modelling. In each cell, *T*-year water depths were estimated empirically from the series of 10 000 simulated water depths. Pluvial flood hazard maps were developed in Pamplona for 10 return periods in the range from two to 500 years, identifying the main pluvial flood hotspots in the urban area.

The stochastic methodology was compared with the standard approach based on *T*-year design storms. Several points at three depressions in Pamplona were selected for the comparison, concluding that both methodologies supply similar results in the control points. However, the stochastic methodology proposed in this paper addresses the drawbacks of the standard approach. First, the stochastic methodology avoids the uncertainties associated with catchment response time estimates with empirical formulae. Second, the stochastic methodology does not need to consider varying storm durations in terms of the catchment response time for each depression and can be easily implemented in multi-depression areas. Third, the assumption that states that the *T*-year storm generates the *T*-year pluvial flood is improved by obtaining the complete probability distribution of water depths in each cell. In addition, bivariate return periods can be estimated, showing that a given *T*-year pluvial flood can be generated by a set of storms with varying combinations of precipitation and duration. Bivariate return-period curves show that precipitation increases with storm duration for a given return period. In a given depression, the slope exhibited by such curves will depend on infiltration rates at its draining catchment. Higher infiltration rates will generate greater rainfall losses and smaller runoff volumes, leading to a higher increase in precipitation with storm duration. Therefore, rural catchments will have steeper bivariate return-period curves than urban catchments.

In this first exploratory analysis, spatially uniform precipitations have been considered. The results are limited by the hydrostatic assumption of the Safer_RAIN tool, identifying water depths only in depressions where runoff water volumes tend to accumulate. However, the stochastic methodology proposed in this study benefits from the reduced computation times required by the fast-processing DEM-based Safer_RAIN algorithm, overcoming the limitations associated with the high computation times required by two-dimensional hydrodynamic models. Therefore, the methodology proposed is a promising technique to develop consistent pluvial flood hazard maps in urban areas at large-scale and multi-depression cities or municipalities.

CRediT authorship contribution statement

Luis Mediero: Conceptualization, Methodology, Data curation, Writing – original draft, Writing – review & editing, Visualization, Investigation, Supervision, Project administration. **Enrique Soriano:** Methodology, Data curation, Visualization, Investigation. **Peio Oria:** Conceptualization, Methodology, Data curation, Writing – original draft, Writing – review & editing, Visualization, Investigation. **Stefano Bagli:** Software, Supervision, Project administration. **Attilio Castellarin:** Conceptualization, Methodology, Software, Writing – original draft, Writing – review & editing, Investigation, Supervision, Project administration. **Luis Garrote:** Conceptualization, Methodology, Investigation, Supervision. **Paolo Mazzoli:** Software, Project administration. **Jaroslav Mysiak:** Methodology, Investigation, Project administration. **Stefania Pasetti:** Software, Project administration. **Simone Persiano:** Methodology, Software, Writing – original draft, Writing – review & editing, Investigation. **David Santillán:** Data curation, Writing – original draft, Writing – review & editing, Investigation. **Kai Schröter:** Methodology, Investigation, Project administration.

Declaration of Competing Interest

The authors declare that they have no known competing financial interests or personal relationships that could have appeared to influence the work reported in this paper.

Acknowledgments

This research was funded by the EIT Climate-KIC Demonstrator project SaferPlaces – Improved assessment of pluvial, fluvial and coastal flood hazards and risks in European cities as a mean to build safer and resilient communities, Task ID: EIT_2.2.37_200246_P401_1B. The SaferPlaces project aims to advice identification and assessment of flood risk mitigation measures and plans, inform climate adaptation and disaster risk reduction strategies, and help to foster multi-stakeholder agreements and partnership for resilience building. It has employed innovative climate, hydrological and hydraulic, topographic and economic modelling techniques to develop the SaferPlaces platform (https://platform.saferplaces.co), in order to assess pluvial, fluvial and coastal flood hazard and risk in urban environments under current and future climates.

The authors would like to acknowledge the Spanish *Instituto*

Geográfico Nacional (IGN) for supplying the 2-m DEM; the SAIH real-time system of the River Ebro Basin Authority, the Spanish *Agencia Estatal de Meteorología* (AEMET), the Regional Government of Navarre and the *Universidad Pública de Navarra* (UPNA) for supplying the precipitation data, and the *Consorcio de Compensación de Seguros* for supplying a database of direct flood losses in Pamplona used to identify the main areas prone to pluvial floods.

The authors also express their gratitude to Andrew Selby for the help and guidance received with regard to language usage and expression.

Appendix A. Supplementary data

Supplementary data to this article can be found online at https://doi.org/10.1016/j.jhydrol.2022.127649.

References

Apel, H., Martínez Trepat, O., Hung, N.N., Chinh, D.T., Merz, B., Dung, N.V., 2016. Combined fluvial and pluvial urban flood hazard analysis: concept development and application to Can Tho city, Mekong Delta, Vietnam. Nat. Hazards Earth Syst. Sci. 16, 941–961. https://doi.org/10.5194/nhess-16-941-2016.

Bates, P.D., Horritt, M.S., Fewtrell, T.J., 2010. A simple inertial formulation of the shallow water equations for efficient two-dimensional flood inundation modelling. J. Hydrol. 387 (1–2), 33–45. https://doi.org/10.1016/j.jhydrol.2010.03.027.

Bennett, N.D., Croke, B.F.W., Guariso, G., Guillaume, J.H.A., Hamilton, S.H., Jakeman, A.J., Marsili-Libelli, S., Newham, L.T.H., Norton, J.P., Perrin, C., Pierce, S. A., Robson, B., Seppelt, R., Voinov, A.A., Fath, B.D., Andreassian, V., 2013. Characterising performance of environmental models. Environ. Model. Softw. 40, 1–20. https://doi.org/10.1016/j.envsoft.2012.09.011.

Berkhahn, S., Fuchs, L., Neuweiler, I., 2019. An ensemble neural network model for real-time prediction of urban floods. J. Hydrol. 575, 743–754. https://doi.org/10.1016/j.jhydrol.2019.05.066.

Bermudez, M., Cea, L., Puertas, J., 2019. A rapid flood inundation model for hazard mapping based on least squares support vector machine regression. J. Flood Risk Manag. 12 (Suppl. 1), e12522 https://doi.org/10.1111/jfr3.12522.

Bermúdez, M., Ntegeka, V., Wolfs, V., Willems, P., 2018. Development and Comparison of Two Fast Surrogate Models for Urban Pluvial Flood Simulations. Water Resour Manage. 32, 2801–2815. https://doi.org/10.1007/s11269-018-1959-8.

Bernini, A., Franchini, M., 2013. A Rapid Model for Delimiting Flooded Areas. Water Resour Manage. 27, 3825–3846. https://doi.org/10.1007/s11269-013-0383-3.

Bladé, E., Cea, L., Corestein, G., Escolano, E., Puertas, J., Vázquez-Cendón, E., Dolz, J., Coll, A., 2014. Iber: herramienta de simulación numérica del flujo en ríos. Rev. Int. Métodos Numér. Cálc. Diseño Ing. 483 (30), 1–10. https://doi.org/10.1016/j.rimni.2012.07.004.

Blanc, J., Hall, J., Roche, N., Dawson, R., Cesses, Y., Burton, A., Kilsby, C., 2012. Enhanced efficiency of pluvial flood risk estimation. J. Flood Risk Manage. 5, 143–152. https://doi.org/10.1111/j.1753-318X.2012.01135.x.

Bruwier, M., Archambeau, P., Erpicum, S., Pirotton, M., Dewals, B., 2017. Shallow-water models with anisotropic porosity and merging for flood modelling on Cartesian grids. J. Hydrol. 554, 693–709. https://doi.org/10.1016/j.jhydrol.2017.09.051.

Bulti, D.T., Abebe, B.G., 2020. A review of flood modeling methods for urban pluvial flood application. Model. Earth Syst. Environ. 6, 1293–1302. https://doi.org/10.1007/s40808-020-00803-z.

Cea, L., Puertas, J., Vázquez-Cendón, M.E., 2007. Depth Averaged Modelling of Turbulent Shallow Water Flow with Wet-Dry Fronts. Arch. Comput. Methods Eng. 14, 303–341. https://doi.org/10.1007/s11831-007-9009-3.

Chang, L.C., Shen, H.Y., Wang, Y.F., Huang, J.Y., Lin, Y.T., 2010. Clustering-based hybrid inundation model for forecasting flood inundation depths. J. Hydrol. 385 (1), 257–268. https://doi.org/10.1016/j.jhydrol.2010.02.028.

Chow, V., Maidment, D., Mays, L., 1988. Applied Hydrology, first ed. McGraw-Hill Science/Engineering/Math, New York, NY, USA.

Chu, X., Yang, J., Chi, Y., Zhang, J., 2013. Dynamic puddle delineation and modeling of puddle-to-puddle filling-spilling-merging-splitting overland flow processes. Water Resour. Res. 49, 3825–3829. https://doi.org/10.1002/wrcr.20286.

Cueto-Felgueoso, L., Santillán, D., García-Palacios, J.H., Garrote, L., 2019. Comparison between 2D Shallow-Water Simulations and Energy-Momentum Computations for Transcritical Flow Past Channel Contractions. Water 11 (7), 1476. https://doi.org/10.3390/w11071476.

Di Baldassarre, G., Schumann, G., Bates, P.D., Freer, J.E., Beven, K.J., 2010. Flood-plain mapping: a critical discussion of deterministic and probabilistic approaches. Hydrol. Sci. J. 55 (3), 364–376. https://doi.org/10.1080/02626661003683389.

Falter, D., Vorogushyn, S., Lhomme, J., Apel, H., Gouldby, B., Merz, B., 2013. Hydraulic model evaluation for large-scale flood risk assessments. Hydrol. Process. 27, 1331–1340. https://doi.org/10.1002/hyp.9553.

Genest, C., Rémillard, B., 2008. Validity of the parametric bootstrap for goodness-of-fit testing in semiparametric models. Ann. I. H. Poincare-Pr. 44, 1096–1127. https://doi.org/10.1214/07-AIHP148.

Genest, C., Rémillard, B., Beaudoin, D., 2009. Goodness-of-fit tests for copulas: A review and a power study. Insur. Math. Econ. 44, 199–213. https://doi.org/10.1016/j.insmatheco.2007.10.005.

Gericke, O.J., Smithers, J.C., 2014. Review of methods used to estimate catchment response time for the purpose of peak discharge estimation. Hydrol. Sci. J. 59 (11), 1935–1971. https://doi.org/10.1080/02626667.2013.866712.

Ghimire, B., Chen, A.S., Guidolin, M., Keedwell, E.C., Djordjević, S., Savić, D.A., 2013. Formulation of a fast 2D urban pluvial flood model using a cellular automata approach. J. Hydroinform. 15 (3), 676–686. https://doi.org/10.2166/hydro.2012.245.

Green, W.H., Ampt, G.A., 1911. Studies on Soil Physics 1, The Flow of Air and Water through Soils. J. Agric. Sci. 4, 1–24. https://doi.org/10.1017/S0021859600001441.

Grimaldi, S., Petroselli, A., Tauro, F., Porfiri, M., 2012. Time of concentration: a paradox in modern hydrology. Hydrol. Sci. J. 57 (2), 217–228. https://doi.org/10.1080/02626667.2011.644244.

Guidolin, M., Chen, A.S., Ghimire, B., Keedwell, E.C., Djordjevic, S., Savic, D.A., 2016. A weighted cellular automata 2D inundation model for rapid flood analysis. Environ. Modell. Softw. 84, 378–394. https://doi.org/10.1016/j.envsoft.2016.07.008.

Guinot, V., Sanders, B.F., Schubert, J.E., 2017. Dual integral porosity shallow water model for urban flood modelling. Adv. Water Resour. 103, 16–31. https://doi.org/10.1016/j.advwatres.2017.02.009.

Henonin, J., Russo, B., Mark, O., Gourbesville, P., 2013. Real-time urban flood forecasting and modelling – a state of the art. J. Hydroinform. 15 (3), 717–736. https://doi.org/10.2166/hydro.2013.132.

Hosking, J.R.M., Wallis, J.R., 1993. Some statistics useful in regional frequency analysis. Water Resour. Res. 29 (2), 271–281.

Hosking, J.R.M., Wallis, J.R., 1997. Regional frequency analysis: an approach based on L-moments. Cambridge University Press, Cambridge, UK.

Hurford, A., Parker, D., Priest, S., Lumbroso, D., 2012. Validating return periods used for Extreme Rainfall Alerts. J. Flood Risk Manage. 5, 134–142. https://doi.org/10.1111/j.1753-318X.2012.01133.x.

Jamali, B., Bach, P.M., Cunningham, L., Deletic, A., 2019. A Cellular Automata fast flood evaluation (CA-ffé) model. Water Resour. Res. 55, 4936–4953. https://doi.org/10.1029/2018WR023679.

Jamali, B., Bach, P.M., Deletic, A., 2020. Rainwater harvesting for urban flood management - An integrated modelling framework. Water Res. 171, 115372 https://doi.org/10.1016/j.watres.2019.115372.

Jhong, B.C., Wang, J.H., Lin, G.F., 2017. An integrated two-stage support vector machine approach to forecast inundation maps during typhoons. J. Hydrol. 547, 236–252. https://doi.org/10.1016/j.jhydrol.2017.01.057.

Kaspersen, P.S., Ravn, N.H., Arnbjerg-Nielsen, K., Madsen, H., Drews, M., 2017. Comparison of the impacts of urban development and climate change on exposing European cities to pluvial flooding. Hydrol. Earth Syst. Sci. 21, 4131–4147. https://doi.org/10.5194/hess-21-4131-2017.

Krvavica, N., Rubinić, J., 2020. Evaluation of Design Storms and Critical Rainfall Durations for Flood Prediction in Partially Urbanized Catchments. Water 12 (7), 2044. https://doi.org/10.3390/w12072044.

Kundzewicz, Z.W., Kanae, S., Seneviratne, S.I., Handmer, J., Nicholls, N., Peduzzi, P., Mechler, R., Bouwer, L.M., Arnell, N., Mach, K., Muir-Wood, R., Brakenridge, G.R., Kron, W., Benito, G., Honda, Y., Takahashi, K., Sherstyukov, B., 2014. Flood risk and climate change: global and regional perspectives. Hydrolog. Sci. J. 59 (1), 1–28. https://doi.org/10.1080/02626667.2013.857411.

Lang, M., Ouarda, T.B.M.J., Bobée, B., 1999. Towards operational guidelines for over-threshold modeling. J. Hydrol. 225, 103–117. https://doi.org/10.1016/S0022-1694(99)00167-5.

Lawrence, D., Paquet, E., Gailhard, J., Fleig, A.K., 2014. Stochastic semi-continuous simulation for extreme flood estimation in catchments with combined rainfall–snowmelt flood regimes. Nat. Hazards Earth Syst. Sci. 14, 1283–1298. https://doi.org/10.5194/nhess-14-1283-2014.

Leandro, J., Chen, A.S., Schumann, A., 2014. A 2D parallel diffusive wave model for floodplain inundation with variable time step (P-DWave). J. Hydrol. 517, 250–259. https://doi.org/10.1016/j.jhydrol.2014.05.020.

Lin, G.F., Lin, H.Y., Chou, Y.C., 2013. Development of a real-time regional-inundation forecasting model for the inundation warning system. J. Hydroinform. 15 (4), 1391–1407. https://doi.org/10.2166/hydro.2013.202.

Mailhot, A., Lachance-Cloutier, S., Talbot, G., Favre, A.C., 2013. Regional estimates of intense rainfall based on the Peak-Over-Threshold (POT) approach. J. Hydrol. 476, 188–199. https://doi.org/10.1016/j.jhydrol.2012.10.036.

Madsen, H., Rasmussen, P.F., Rosbjerg, D., 1997. Comparison of annual maximum series and partial duration series methods for modeling extreme hydrologic events: 1. At-site modeling, Water Resour. Res. 33 (4), 747–757. https://doi.org/10.1029/96WR03848.

Marshall, J.S., Palmer, W.M., 1948. The distribution of raindrops with size. J. Meteor. 5, 165–166.

Martins, E.S., Stedinger, J.R., 2001. Generalized Maximum Likelihood Pareto-Poisson estimators for partial duration series. Water Resour. Res. 37 (10), 2551–2557. https://doi.org/10.1029/2001WR000367.

McKee, J.L., Binns, A.D., 2016. A review of gauge–radar merging methods for quantitative precipitation estimation in hydrology. Can. Water Resour. J. 41 (1–2), 186–203. https://doi.org/10.1080/07011784.2015.1064786.

Mediero, L., Jiménez-Álvarez, A., Garrote, L., 2010. Design flood hydrographs from the relationship between flood peak and volume. Hydrol. Earth Syst. Sci. 14, 2495–2505. https://doi.org/10.5194/hess-14-2495-2010.

Neal, J., Fewtrell, T., Trigg, M., 2009. Parallelisation of storage cell flood models using OpenMP. Environ. Modell. Softw. 24, 872–877. https://doi.org/10.1016/j.envsoft.2008.12.004.

Néelz, S., Pender, G., 2007. Sub-grid scale parameterisation of 2D hydrodynamic models of inundation in the urban area. Acta Geophys. 55, 65–72. https://doi.org/10.2478/s11600-006-0039-2.

NRCS, 2010. Time of concentration. National Engineering Handbook. Part 630 Hydrology. Chapter 15. Natural Resources Conservation Service.
Nuswantoro, R., Diermanse, F., Molkenthin, F., 2016. Probabilistic flood hazard maps for Jakarta. J. Flood Risk Manage. 9, 105–124. https://doi.org/10.1111/jfr3.12114.
Ochoa-Rodriguez, S., Wang, L.P., Willems, P., Onof, C., 2019. A review of radar-rain gauge data merging methods and their potential for urban hydrological applications, Water Resour. Res. 55, 6356–6391. https://doi.org/10.1029/2018WR023332.
Palla, A., Colli, M., Candela, A., Aronica, G., Lanza, L., 2018. Pluvial flooding in urban areas: the role of surface drainage efficiency. J. Flood Risk Manage. 11, S663–S676. https://doi.org/10.1111/jfr3.12246.
Pan, T.Y., Lai, J.S., Chang, T.J., Chang, H.K., Chang, K.C., Tan, Y.C., 2011. Hybrid neural networks in rainfall-inundation forecasting based on a synthetic potential inundation database. Nat. Hazards Earth Syst. Sci. 11, 771–787. https://doi.org/10.5194/nhess-11-771-2011.
Requena, A.I., Mediero, L., Garrote, L., 2013. A bivariate return period based on copulas for hydrologic dam design: accounting for reservoir routing in risk estimation. Hydrol. Earth Syst. Sci. 17, 3023–3038. https://doi.org/10.5194/hess-17-3023-2013.
Salvadori, G., De Michele, C., 2011. Estimating strategies for multiparameter Multivariate Extreme Value copulas. Hydrol. Earth Syst. Sci. 15, 141–150. https://doi.org/10.5194/hess-15-141-2011.
Samela, C., Persiano, S., Bagli, S., Luzzi, V., Mazzoli, P., Humer, G., Reithofer, A., Essenfelder, A., Amadio, M., Mysiak, J., Castellarin, A., 2020. Safer_RAIN: A DEM-Based Hierarchical Filling-&-Spilling Algorithm for Pluvial Flood Hazard Assessment and Mapping across Large Urban Areas. Water 12, 1514. https://doi.org/10.3390/w12061514.
Santillán, D., Cueto-Felgueoso, L., Sordo-Ward, A., Garrote, L., 2020. Influence of Erodible Beds on Shallow Water Hydrodynamics during Flood Events. Water 12 (2), 3340. https://doi.org/10.3390/w12123340.
Shapiro, A., Willingham, K.M., Potvin, C.K., 2010. Spatially Variable Advection Correction of Radar Data. Part I: Theor. Consider., J. Atmospheric Sci. 67 (11), 3445–3456. https://doi.org/10.1175/2010JAS3465.1.
Sharon, A.J., Gaussiat, N., 2015. An assessment of kriging-based rain- gauge–radar merging techniques. Q. J. Roy. Meteor. Soc. 141 (691), 2300–2313. https://doi.org/10.1002/qj.2522.
Simões, N.E., Ochoa-Rodríguez, S., Wang, L.P., Pina, R.D., Marques, A.S., Onof, C., Leitão, J.P., 2015. Stochastic Urban Pluvial Flood Hazard Maps Based upon a Spatial-Temporal Rainfall Generator. Water 7, 3396–3406. https://doi.org/10.3390/w7073396.
Sklar, A., 1959. Fonctions de rèpartition à n dimensions et leurs marges. Publ. Inst. Stat. Univ. Paris 8, 229–231.
Stedinger, J.R., Vogel, R.M., Foufoula-Georgiou. (1992) Frequency analysis of extreme events. In: 'Handbook of Hydrology', Chapter 18. Ed. D. R. Maidment, McGraw-Hill.
Tabary, P., 2007. The New French Operational Radar Rainfall Product. Part I: Methodology. Weather Forecasting 22 (3), 393–408. https://doi.org/10.1175/WAF1004.1.
Teng, J., Jakeman, A.J., Vaze, J., Croke, B.F.W., Dutta, D., Kim, S., 2017. Flood inundation modelling: A review of methods, recent advances and uncertainty analysis. Environ. Modell. Softw. 90, 201–216. https://doi.org/10.1016/j.envsoft.2017.01.006.
Tuyls, D.M., Thorndahl, S., Rasmussen, M.R., 2018. Return period assessment of urban pluvial floods through modelling of rainfall–flood response. J. Hydroinform. 20 (4), 829–845. https://doi.org/10.2166/hydro.2018.133.
Yu, D. and Lane, S. N. (2006) Urban fluvial flood modelling using a two-dimensional diffusion-wave treatment, part 2: development of a sub-grid-scale treatment. Hydrol. Process., 20, 1567-1583, 0.1002/hyp.5936.
Zhang, J., Howard, K., Langston, C., Kaney, B., Qi, Y., Tang, L., Grams, H., Wang, Y., Cocks, S., Martinaitis, S., Arthur, A., Cooper, K., Brogden, J., Kitzmiller, D., 2016. Multi-Radar Multi-Sensor (MRMS) Quantitative Precipitation Estimation: Initial Operating Capabilities. B. Am. Meteorol. Soc. 97 (4), 621–638. https://doi.org/10.1175/BAMS-D-14-00174.1.
Zhang, S., Pan, B., 2014. An urban storm-inundation simulation method based on GIS. J. Hydrol. 517, 260–268. https://doi.org/10.1016/j.jhydrol.2014.05.044.
Zhang, S., Wang, T., Zhao, B., 2014. Calculation and visualization of flood inundation based on a topographic triangle network. J. Hydrol. 509, 406–415. https://doi.org/10.1016/j.jhydrol.2013.11.060.